NNT/NL : 2020AIXM0001/001ED000

Habilitation à Diriger des Recherches

Présentée à Aix-Marseille Université

le XX janvier 2022 par

Julián Ernesto BAUTISTA

Dark-energy with Spectroscopic Observations of the Universe

Discipline
Physique et Sciences de la Matière

Spécialité
Astrophysique et Cosmologie

Laboratoire
Centre de Physique des Particules de Marseille

Composition du jury

Prénom NOM Affiliation	Rapporteur·e
Prénom NOM Affiliation	Rapporteur·e
Prénom NOM Affiliation	Examinateur·rice
Prénom NOM Affiliation	Président·e du jury
Prénom NOM Affiliation	Tuteur

Je soussigné, [Prénom Nom], déclare par la présente que le travail présenté dans ce manuscrit est mon propre travail, réalisé sous la direction scientifique de [Prénom Nom], dans le respect des principes d'honnêteté, d'intégrité et de responsabilité inhérents à la mission de recherche. Les travaux de recherche et la rédaction de ce manuscrit ont été réalisés dans le respect à la fois de la charte nationale de déontologie des métiers de la recherche et de la charte d'Aix-Marseille Université relative à la lutte contre le plagiat.

Ce travail n'a pas été précédemment soumis en France ou à l'étranger dans une version identique ou similaire à un organisme examinateur.

Fait à [ville] le [date]

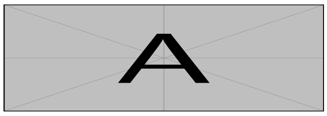

Résumé

Lorem ipsum dolor sit amet, consectetuer adipiscing elit. Ut purus elit, vestibulum ut, placerat ac, adipiscing vitae, felis. Curabitur dictum gravida mauris. Nam arcu libero, nonummy eget, consectetuer id, vulputate a, magna. Donec vehicula augue eu neque. Pellentesque habitant morbi tristique senectus et netus et malesuada fames ac turpis egestas. Mauris ut leo. Cras viverra metus rhoncus sem. Nulla et lectus vestibulum urna fringilla ultrices. Phasellus eu tellus sit amet tortor gravida placerat. Integer sapien est, iaculis in, pretium quis, viverra ac, nunc. Praesent eget sem vel leo ultrices bibendum. Aenean faucibus. Morbi dolor nulla, malesuada eu, pulvinar at, mollis ac, nulla. Curabitur auctor semper nulla. Donec varius orci eget risus. Duis nibh mi, congue eu, accumsan eleifend, sagittis quis, diam. Duis eget orci sit amet orci dignissim rutrum.

Mots clés: géométrie algorithmique, complexe planaire et rectangulaire, géodésique, courbure globale non-positive

Abstract

Lorem ipsum dolor sit amet, consectetuer adipiscing elit. Ut purus elit, vestibulum ut, placerat ac, adipiscing vitae, felis. Curabitur dictum gravida mauris. Nam arcu libero, nonummy eget, consectetuer id, vulputate a, magna. Donec vehicula augue eu neque. Pellentesque habitant morbi tristique senectus et netus et malesuada fames ac turpis egestas. Mauris ut leo. Cras viverra metus rhoncus sem. Nulla et lectus vestibulum urna fringilla ultrices. Phasellus eu tellus sit amet tortor gravida placerat. Integer sapien est, iaculis in, pretium quis, viverra ac, nunc. Praesent eget sem vel leo ultrices bibendum. Aenean faucibus. Morbi dolor nulla, malesuada eu, pulvinar at, mollis ac, nulla. Curabitur auctor semper nulla. Donec varius orci eget risus. Duis nibh mi, congue eu, accumsan eleifend, sagittis quis, diam. Duis eget orci sit amet orci dignissim rutrum.

Keywords: computational geometry, planar and rectangular complex, geodesic, global nonpositive curvature

Acknowledgements

Le modèle de thèse AMU n'existerait pas sans la contribution des doctorants. Nous souhaitons remercier tout particulièrement Mickaël Bojados, Flora Cordoleani et Florian Caullery pour leur aide précieuse et la qualité de leurs fichiers sources LaTeX. La mise à jour effectuée en 2018 doit beaucoup à l'excellent travail de Dorian Depriester.

Lorem ipsum dolor sit amet, consectetuer adipiscing elit. Ut purus elit, vestibulum ut, placerat ac, adipiscing vitae, felis. Curabitur dictum gravida mauris. Nam arcu libero, nonummy eget, consectetuer id, vulputate a, magna. Donec vehicula augue eu neque. Pellentesque habitant morbi tristique senectus et netus et malesuada fames ac turpis egestas. Mauris ut leo. Cras viverra metus rhoncus sem. Nulla et lectus vestibulum urna fringilla ultrices. Phasellus eu tellus sit amet tortor gravida placerat. Integer sapien est, iaculis in, pretium quis, viverra ac, nunc. Praesent eget sem vel leo ultrices bibendum. Aenean faucibus. Morbi dolor nulla, malesuada eu, pulvinar at, mollis ac, nulla. Curabitur auctor semper nulla. Donec varius orci eget risus. Duis nibh mi, congue eu, accumsan eleifend, sagittis quis, diam. Duis eget orci sit amet orci dignissim rutrum.

Nam dui ligula, fringilla a, euismod sodales, sollicitudin vel, wisi. Morbi auctor lorem non justo. Nam lacus libero, pretium at, lobortis vitae, ultricies et, tellus. Donec aliquet, tortor sed accumsan bibendum, erat ligula aliquet magna, vitae ornare odio metus a mi. Morbi ac orci et nisl hendrerit mollis. Suspendisse ut massa. Cras nec ante. Pellentesque a nulla. Cum sociis natoque penatibus et magnis dis parturient montes, nascetur ridiculus mus. Aliquam tincidunt urna. Nulla ullamcorper vestibulum turpis. Pellentesque cursus luctus mauris.

Contents

Résumé 3

Abstract 4

Acknowledgements 5

Contents 6

1 Introduction 8
- 1.1 The history of our Universe and its big open questions . . . 8
- 1.2 Evidences for the accelerated expansion of the Universe . . . 9
- 1.3 Model of an expanding Universe . . . 10
  - 1.3.1 Assumptions and ingredients . . . 10
  - 1.3.2 The expansion rate . . . 10
  - 1.3.3 Distances in cosmology . . . 11
  - 1.3.4 Dark-energy models . . . 12
- 1.4 Model of the large-scale structures . . . 12
  - 1.4.1 Statistical description of perturbations . . . 13
  - 1.4.2 Configuration and Fourier space . . . 14
  - 1.4.3 Cosmological dependency of the power spectrum . . . 14
  - 1.4.4 The amplitude of the power spectrum . . . 15
- 1.5 Cosmological probes of expansion . . . 16
  - 1.5.1 Direct measurements of H_0 . . . 16
  - 1.5.2 Type-Ia supernovae . . . 17
  - 1.5.3 Big Bang nucleosynthesis . . . 18
  - 1.5.4 Baryon acoustic oscillations . . . 19
  - 1.5.5 The cosmic microwave background . . . 20
  - 1.5.6 Redshift-space distortions . . . 21
  - 1.5.7 Weak gravitational lensing . . . 23

2 Observing the Universe with spectroscopy 24
- 2.1 Selecting the objects to observe . . . 24
- 2.2 Pointing fibres to the sky . . . 25
- 2.3 From electrons to spectra . . . 26
- 2.4 From spectra to redshifts . . . 28
- 2.5 From redshifts to cosmology . . . 28

3 The high-redshift Universe and its forests 29
- 3.1 Forests as a tracer of the Universe's structures . . . 29
- 3.2 Baryon acoustic oscillations in the forests . . . 31
  - 3.2.1 Transmission field . . . 32
  - 3.2.2 Two-point correlation functions . . . 33

3.2.3 Correction matrices . . . 34
3.2.4 BAO model . . . 34
3.3 Impact of redshift errors . . . 34
3.4 Weak-lensing of forests . . . 34

4 The mid-redshift Universe and its galaxies **35**
4.1 Galaxies as a tracer of the matter field . . . 35
4.2 Baryon acoustic oscillations with galaxies . . . 35
4.3 Redshift-space distortions . . . 35
4.4 Cross-correlation with radio surveys . . . 35

5 The low-redshift Universe and its velocities **36**
5.1 Measuring peculiar velocities . . . 36
5.2 Combining velocities with densities . . . 36
5.3 Testing general relativity with velocities . . . 36

Conclusion **37**

Bibliography **38**

1 Introduction

Contents

1.1 The history of our Universe and its big open questions 8
1.2 Evidences for the accelerated expansion of the Universe 9
1.3 Model of an expanding Universe 10
1.3.1 Assumptions and ingredients 10
1.3.2 The expansion rate 10
1.3.3 Distances in cosmology 11
1.3.4 Dark-energy models 12
1.4 Model of the large-scale structures 12
1.4.1 Statistical description of perturbations 13
1.4.2 Configuration and Fourier space 14
1.4.3 Cosmological dependency of the power spectrum 14
1.4.4 The amplitude of the power spectrum 15
1.5 Cosmological probes of expansion 16
1.5.1 Direct measurements of H_0 16
1.5.2 Type-Ia supernovae 17
1.5.3 Big Bang nucleosynthesis 18
1.5.4 Baryon acoustic oscillations 19
1.5.5 The cosmic microwave background 20
1.5.6 Redshift-space distortions 21
1.5.7 Weak gravitational lensing 23

1.1 The history of our Universe and its big open questions

If we gather all knowledge in physics humanity could learn to this day, we can build an interesting story for how our Universe evolved since *very* early times. This great story that can explain most of what we observe in the sky, while being consistent with experimental results here on Earth. However, this story has several weak spots. Either because where we do not have a satisfactory physical explanation for what we observe, or because we simply cannot observe what happens by then (and potentially we never will).

The story in a nutshell goes as follows: the "beginning" of the Universe[1], also known as the *Big Bang* or *inflation*, was an epoch of exponential expansion of space that happened around 13.8 billion years ago. Inflation transformed quantum, microscopic fluctuations of space into macroscopic density fluctuations of the Universe's constituents: quarks, photons,

[1] The actual beginning of the Universe can be seen as a complex phylosophical question or simply as an ill defined physical concept. This discussion is clearly beyond the scope of this work and/or my capabilities. Here, I decide to name as beginning the first epoch of the Universe for which we have a widely known physical theory to describe it.

neutrinos and dark-matter. After inflation, the Universe continues to expand but much slowly. The average temperature of the Universe decreases adiabatiacally. Quarks start to gather to form protons, neutrons and relics of heavier atoms, such as deuterium, tritium, helium, litium and so on. All this during the first few minutes of the Universe's history, in the so called *Big Bang nucleosynthesis*. After 380 thousand years, electrons rebind with protons to form neutral hydrogen, and photons scatter for their last time with them as the Universe becomes more difuse. The photons from this epoch are observable today and are known as the *cosmic microwave background*. The Universe goes through its *dark ages*, where hydrogen is mostly neutral and stars have not yet formed. After several million years, gravity clumps hydrogen into dense clouds that reach high enough temperatures to start thermonuclear reactions in their core. The first stars are formed. Then the first galaxies. These galaxies merge into larger galaxies, galaxies form small virialized groups, large groups, clusters, super clusters. Clusters, filamentary structures and voids compose the so called cosmic web. At around half of the Universe's age, the expansion starts to speed up again, accelerating, as if gravity became repulsive on very large scales. Then, on one of the many billions of galaxies, the *Milky Way*, planet Earth formed around a somewhat isolated star, the Sun, and here we are today, observing the sky, trying to explain the whole Universe.

This story is based on the assumption that general relativity (GR) is the theory of gravity, that the Universe can be modelled as statistically homogeneous and isotropic on large enough scales, and that the Universe is composed of the standard model particles and interactions, with the addition of two exotic components: dark-energy and dark-matter.

The physical origin of dark-energy and dark-matter is a mystery and one of the weak spots of the Universe's story. Another weak spot is the physics of inflation, but observables related to that time are limited. [Any others ?] Solutions for these problems would represent major breakthroughts in physics and large teams of scientists are dedicated to them, either theoretically or experimentally.

My past work has been focused on the observations related to dark-energy. The rest of this chapter will be dedicated to explaining the problem of accelerated expansion, the dark-energy model and other possible solutions, and how do we observe the expansion.

1.2 Evidences for the accelerated expansion of the Universe

Not long after developing his theory of gravity, Einstein wanted to write a model for a static Universe filled with matter. Since gravity is attractive, his solution was to include a new constant term, Λ, in the equations. This will be later known as the *cosmological constant*, one of the simplest models of dark-energy in agreement with a wide variety of cosmological observations.

The first indirect evidences for dark-energy come from measurements of galaxy clustering in the 80's (Maddox et al. 1990; Efstathiou et al. 1990). At the end of the 90's, two independent teams measured the expansion of the Universe using type-Ia supernovae (Riess, Filippenko, et al. 1998; Perlmutter et al. 1999). Their observations could only be explained by an Universe containing around 30 per cent of matter and 70 per cent of dark energy, in the form of a cosmological constant. Few years later, first measurements of the temperature fluctuations in the cosmic microwave background were consistent with an Universe with a flat space (Balbi et al. 2000; de Bernardis et al. 2000), which in combination with measurements of clustering, supernovae and the local expansion rate (Mould et al. 2000), definitely confirmed that the Universe's expansion is accelerating. Age estimates of globular stellar clusters, which are supposed to be among the oldest astrophysical objects, were also indicating that the Universe had to be older than the age predicted by models of an Universe only filled with matter (Chaboyer 1998). The following decade was enriched by the first measurements of the baryon acoustic oscillations in the distribution of galaxies (Eisenstein, Zehavi, et al. 2005; Cole et al. 2005), re-confirming the accelerated nature of the expansion.

Since the 2010's, we live in the so-called *precision cosmology* era, where several observatories were constructed with the main goal of improving the precision of all these measurements just discussed. Even with the most up-to-date results, with errors of the order of a few percent, there is yet no evidence for a departure from the model of Universe governed by GR, composed by 70 per cent of this mysterious cosmological constant and by 25 per cent by this mysterious dark-matter.

1.3 Model of an expanding Universe

1.3.1 Assumptions and ingredients

In order to define some important cosmological parameters, I will quickly review the basics of the current most accepted model for our Universe in the limit of very large scales, where it can be considered homogenous and isotropic. This is also knwon as the *background* model, since the formation of structures (see next section) can be modeled as small perturbations around it. It is also assumed that gravity is described by general relativity, which interlinks the fabric of space-time and energy densities of the Universe constituents. For these constituents, we assume the presence of *baryons* (protons, electrons, atoms), photons, neutrinos, cold dark-matter and dark-energy.

The expansion of space is usually parametrised by the scale factor $a(t)$, a function of time t that dictates how physical and comoving distances relate to each other. We assume that $a(t_0) = 1$ today ($t_0 = 13.8$ Gyr) and that $a \to 0$ as $t \to 0$. The speed of the expansion and its acceleration are simply derivatives with respect to time, $\dot{a}(t)$ and $\ddot{a}(t)$, respectively. The expansion rate of the Universe is defined as $H(t) = \dot{a}(t)/a(t)$ and takes the Hubble constant value today, $H(t_0) = H_0 = 100h$ km/s/Mpc ~ 70 km/s/Mpc. Since the scale factor is a monotonically increasing function of time (in our simple model), a is commonly used to describe a given cosmic epoch.

One of the consequences of the expansion is that relativistic species, such as photons and massless neutrinos, loose energy or are *redshifted* as they propagate. In astronomy, the redshift z is defined as the relative difference in wavelength between the one emmited by source and the one observed. Thus, in an expanding Universe the scale factor is related to the redshift as $a = 1/(1+z)$. Redshift is also commonly used to describe cosmic epoch or distances. Today corresponds to $z = 0$ while $z \to \infty$ as $t \to 0$.

1.3.2 The expansion rate

The expansion rate can be derived from GR equations and be written as a function of redshift and the densities of each consituent

$$H^2(z) = H_0^2 \left[\Omega_m (1+z)^3 + \Omega_r (1+z)^4 + \Omega_{de}(z) + \Omega_k (1+z)^2\right] \tag{1.1}$$

where $\Omega_x = \rho_x/\rho_{\text{crit}}$ is the ratio between the density constituent x today and the critical energy density $\rho_{\text{crit}} = 3H_0^2/8\pi G$, which is the density required for a flat space geometry. The subscripts m, r, de and k stand for non-relativistic species (baryons, cold dark-matter and non-relativistic neutrinos), relativistic species (photons and relativistic neutrinos), dark-energy and curvature, respectively. The curvature "density" parameter is defined as a function of the others, $\Omega_k = (1 - \sum_x \Omega_x)$, and it is zero in a flat space geometry. Non-relativistic species dilute in an expanding universe so their energy density is proportional to $a^{-3} = (1+z)^3$. Relativistic species dilute as well but have an extra factor of a^{-1} due to redshifting. Dark-energy is written as a general function of redshift. In the simplest case of a cosmological constant, $\Omega_{de}(z) = \Omega_\Lambda$, i.e. a constant. The dependency of curvature with a^{-2} simply comes from the field equations.

1.3.3 Distances in cosmology

Distances are non-trivially defined in an expanding, potentially non-flat, Universe. Therefore, different types of distances are more appropriate for certain observables. The *Hubble distance* is related to the expansion rate as

$$D_H(z) = \frac{c}{H(z)}, \tag{1.2}$$

and it is commonly used in measurements of baryon acoustic oscillations in the line-of-sight direction (see Chapters 3 and 4) or to represent the size of a causally connected region of the Universe.

The *comoving distance* to an object at redshift z is written as

$$D_C(z) = \int_0^z \mathrm{d}z' \, D_H(z'). \tag{1.3}$$

This expression yields the distance travelled by a photon from a source towards us but factoring out the scale factor, effectively "removing" the effect of expansion.

The *comoving angular diameter distance* $D_M(z)$ is useful when distances are inferred from angles, which are affected by the curvature of space. An object with comoving size l at a redshift z would be seen with an angular size θ. This allows us to define $D_M(z) = l/\theta(z)$ as

$$D_M(z) = D_C(z)\mathrm{sinc}\left(\sqrt{-\Omega_k}\frac{D_C(z)}{D_H(z=0)}\right), \tag{1.4}$$

where $\mathrm{sinc}(x) = \sin(x)/x$. This distance is used in observations of graviational lensing and in measurements of the baryon acoustic oscillations in the transverse direction to the line-of-sight.

Analogouly, the *luminosity distance* $D_L(z)$ relates the flux f received by an object at redshift z with intrinsic luminosity L. We define then $D_L(z) = \sqrt{L/4\pi f(z)}$ as

$$D_L(z) = D_M(z)(1+z). \tag{1.5}$$

This distance is used in supernova cosmology, where fluxes are used to infer dark-energy properties. Since supernovae fluxes vary by orders of magnitude, it is handy to define the *distance modulus* as the logarithm of the luminosity distance:

$$\mu(z) = 5\log_{10}\frac{D_L(z)}{10\ \mathrm{pc}}. \tag{1.6}$$

This definition is such that it agrees with the definition of magnitude of an object.

In all the distances defined above, the dependency to the cosmological energy densities Ω_x

happens only through $H(z)$ (Eq. 1.1). This is how we can constrain these parameters through distance measurements. However, all cosmological distance measurements are *relative*, which means they are defined to an arbitrary normalisation[2]. It is only by observing the *evolution* of these relative distance measurements as a function of redshift that we can constrain cosmological parameters. Note that in all the distances defined above, the dependency with H_0 only impacts this arbitrary normalisation, so it cannot be measured directly. It is useful to factor out this dependency with H_0, and write distances in units of h^{-1}Mpc (numerically equivalent to set $H_0 = 100$ km/s/Mpc). These are the units used in all works studying the large-scale structures and it is also used thoughout this manuscript.

1.3.4 Dark-energy models

In the Eq. 1.1 for the expansion rate of the Universe, the dark-energy density term is written as a general function of redshift. As mentioned before, the simplest model is to consider a cosmological constant $\Omega_{de}(z) = \Omega_\Lambda$. The cosmological constant can be thought as equivalent to a fluid with relativistic pressure $p_{de} = -\rho_{de}$. This model can be extended by considering a different equation of state $p_{de} = p_{de}(\rho_{de}) = w(z)\rho_{de}$, where $w(z)$ can be a constant or a more general function of redshift, under the condition that $w(z) < -1/3$, needed to obtain an accelerated expansion in a dark-energy dominated Universe. One widely known parametrisation is given by $w(a) = w_0 + w_a(1-a)$ (Chevallier et al. 2001; Linder 2003).

The litterature contains a huge variety of models that attempt to be more physically motivated that those just presented (see Weinberg et al. 2013, section 2.2 for a review). Some of them suggest that maybe general relativity breaks down on large enough scales, causing the expansion to accelerate. They suggest extensions or modifications to Einstein's theory of general relativity, and are commonly known as *modified gravity* models.

1.4 Model of the large-scale structures

The Universe is clearly not homogenous and isotropic. Matter clustered under the influence of gravity, creating the cosmic web, composed of clusters, filaments, empty regions. The model described in the previous section only describes the Universe as a whole, without any inhomogeneities. If we want to describe the evolution of the structures we need to consider an extension to the background model.

Observations of the large-scale structures and the cosmic microwave background (CMB) indicate that the matter density field today is the evolution of tiny density perturbations from the early Universe. Temperature fluctuations in the CMB are of the order of 10^{-5}, while densities today can reach values several orders of magnitude larger than the average density. The most widely accepted theory is that the CMB fluctuations, and today's structures, are originated from the inflation-grown quantum fluctuations, that evolved under the influence of gravity and pressure in the hot dense plasma-like epoch of our Universe.

It is been possible to model the physics of the evolution of these tiny fluctuations using *linear perturbation theory*. The predictions of this theory are an excellent match to observations of the CMB and to the late-time distribution of matter on large scales, i.e., larger than few tens of Mpc. On smaller scales however, gravity becomes highly non-linear and more advanced calculations

[2] Two exceptions are parallax distances which are an absolute measurements based on the known distance between the Earth and the Sun and gravitational wave distances, which amplitudes depend on the distance and on the masses of the progenitors, though the masses affect the wave form as well, breaking the degeneracy.

are required. There are two main approaches to model non-linearities: theoretical calculations going beyond linear terms in perturbation theory or numerical n-body simulations. [Develop?]

The main idea of perturbation theory is to consider that the density of a given species x is given by:

$$\rho_x(\vec{x},t) = \bar{\rho}_x(t)\,[1+\delta_x(\vec{x},t)]\,, \tag{1.7}$$

where the bar indicates average over the whole Universe and $\delta_x \ll 1$ is a small perturbation. The average density $\bar{\rho}_x$ follows the background evolution described in section 1.3. A new set of equations can be derived for the evolution of δ_x for each species depending if x denotes relativitic species (photons, hot baryons, hot neutrinos) or non-relativistic species (cold baryons, cold neutrinos or dark-matter). Only some families of models also consider fluctuations in the dark-energy density.

The evolution of δ_x for a given species is dictated by both Boltzmann and Einstein's GR equations. Boltzmann equations describe the evolution of phase-space distributions of each constituent, considering collisions (pressure) and particle creation and anihilation. GR equations describe how each species influence graviational potentials which in turn make perturbations grow.

Another important ingredient in these equations is the *peculiar velocities* $\vec{v}_x(\vec{x},t)$ of each species, particularly the non-relativistic ones since relativistic species are assumed to have $v \sim c$. They influence the evolution of perturbations through Boltzmann, Euler and continuity equations. These velocities are observable and are an important probe of the cosmological model and on the strength of gravity itself. They will be a key actor in Chapters 4 and 5.

1.4.1 Statistical description of perturbations

The value of the matter density field at a given position $\vec{x}$ is hardly observable and therefore does not contain much cosmological information, since it is just the evolution of a single random realisation of the initial conditions. In cosmology we are mostly interested by the statistical properties of the density field, or of its perturbations. Particularly, most cosmological information is contained in the first moments of the density field, starting from the two-point function (the one-point function is zero by definition), which is defined as

$$\xi(\vec{x},\vec{y}) = \langle \delta(\vec{x})\delta(\vec{y})\rangle \tag{1.8}$$

where $\langle\cdot\rangle$ denotes an ensemble average. Given that we only have one single realisation of the Universe, we assume that averages over space (in an infinite space) are equivalent to ensemble averages.

The assumptions of homogeneity and isotropy of the background can be applied in an statistical sense to the perturbations. Statistical homogeneity makes ξ not to depend on the specific locations $\vec{x}$ and $\vec{y}$ but only on their separation $\vec{r} = \vec{y} - \vec{x}$. Statistical isotropic makes ξ no longer depend on the orientation of $\vec{r}$, only on its absolute value $r = |\vec{r}|$. Therefore, the two-point correlation function simplifies to a function of r:

$$\xi(r) = \langle \delta(\vec{x})\delta(\vec{x}+\vec{r})\rangle. \tag{1.9}$$

The correlation function $\xi(r)$ is a powerful observable which can be compared to predictions from a given cosmological model.

1.4.2 Configuration and Fourier space

The time evolution of linear density perturbations $\delta(\vec{x})$ is dictated by a set of second-order differential equations, containing derivatives with respect to time and space. It is thus convient to apply Fourier transforms to these equations, where derivatives with respect to space become simple products. Separations $\vec{r}$ in the so-called *Configuration space* become wavevectors $\vec{k}$ in *Fourier space*. The density perturbations in Fourier space are defined by

$$\tilde{\delta}(\vec{k}) = \int \mathrm{d}^3 x\, \mathrm{e}^{-i\vec{k}\cdot\vec{x}} \delta(\vec{x}), \tag{1.10}$$

and its inverse is

$$\delta(\vec{x}) = \frac{1}{(2\pi)^3} \int \mathrm{d}^3 k\, \mathrm{e}^{+i\vec{k}\cdot\vec{x}} \tilde{\delta}(\vec{k}). \tag{1.11}$$

As previously, we are interested in the two (or more) point functions of the field. In Fourier space, the two-point correlation function is known as the *power spectrum* and is defined as

$$\left\langle \tilde{\delta}(\vec{k})\tilde{\delta}(\vec{k})' \right\rangle = (2\pi)^3 P(k) \delta^3_{\mathrm{Dirac}}(\vec{k} - \vec{k}'), \tag{1.12}$$

where $\delta^3_{\mathrm{Dirac}}(\vec{x})$ is a three-dimensional Dirac distribution. The assumption of spatial homogeneity is guaranteed by the properties of Fourier space, while the assumption of isotropy makes the power spectrum to be only a function of the absolute value of the wavevector $k = |\vec{k}|$.

When considering the evolution of perturbations in Fourier space to the linear level, each mode $\tilde{\delta}(\vec{k})$ evolves independently of the others. We often say that there is no *mode coupling* in linear theory.

The power spectrum $P(k)$ is an observable, as powerful as the correlation function, to constrain cosmological models. While in theory these two contain exactly the same compressed statistical information, in pratice the analyses of real data use different finite ranges of scales which are affected differently by systematic effects. Therefore, analyses of real data in configuration and Fourier space complement each other. Such analyses are presented in Chapter 4.

1.4.3 Cosmological dependency of the power spectrum

The power spectrum $P(k)$, or the correlation function $\xi(r)$, of density perturbations are an excellent probe of the cosmological model. It encodes information accumulated of the whole Universe's history, since the Big Bang until today.

At the end of inflation, we think that perturbations were roughly Gaussian (as are quantum fluctuations of the vacuum), having a nearly scale independent power spectrum defined by

$$P_0(k) = A_s k^{n_s - 1}, \tag{1.13}$$

where $A_s \sim 2 \times 10^{-9}$ is the amplitude of scalar perturbations and $n_s \sim 0.96$ is the scalar spectral index. The term scalar refers to standard density (or gravitational potential) perturbations, while tensorial perturbations (of the space-time metric) refer to primordial gravitational waves. Vectorial perturbations decay and rapidly become negligible in most common cosmological models.

After inflation, the majority of the energetic budget of Universe was held by photons and neutrinos. Since their energy density decays as a^{-4}, their contribution quickly drops. This radiation-dominated era lasted until $z \sim 5000$, or $t \sim 20$ kyr, when the energy density of matter became the dominant source. Matter density decays at a slower rate, proportional to a^{-3}. Dark-energy became dominant at $z \sim 0.5$, or $t \sim 9$ Gyr, since its energy density is constant (or close to constant). The actual duration of each era depends on relative values of the energy densities, parametrised by Ω_x (see 1.3).

Add figure Matter perturbations grew at different rates during these different eras. In radiation-dominated era, large-scale modes (large values of r or small values of k) grew while small-scale ones oscillated, due to battle between gravity and radiative pressure. These are known as *baryon acoustic oscillations*. These oscillations are imprinted in the power spectrum of the photon-baryon fluid, at the time of the CMB, and in the matter power spectrum at later times. The radiative pressure prohibited the growth of small-scale perturbations, so the matter power spectrum is damped, which results in this hill-like shape. In the matter-dominated era, the radiative pressure becomes negligible and all modes grow equally (neglecting non-linear growth). When dark-energy is dominant, the expansion accelerates and growth of structures slows down slightly.

Well after recombination, matter (baryons + dark) density perturbations obey the following differential equation, if we assume GR and linear theory:

$$\ddot{\delta}(\vec{x}, t) + 2H(z)\dot{\delta}(\vec{x}, t) - \frac{3}{2}\Omega_m H_0^2 (1+z)^3 \delta(\vec{x}, t) = 0. \tag{1.14}$$

If we assume that $\delta(\vec{x}, t) = \delta(\vec{x}, t_0) G(t)/G(t_0)$, we can factor out the spatial dependency and only solve for the time-dependent term $G(t)$, known as the *growth factor*. Its logarithmic derivative with respect to the scale factor $a(t)$ is called *growth rate* of structures:

$$f(a) \equiv \frac{\mathrm{d}\ \ln G(a)}{\mathrm{d}\ \ln a}, \tag{1.15}$$

which is a key observable for which the predicted value depends on the cosmological parameters and on the assumed theory of gravity (e.g., GR in Eq. 1.14).

In linear theory, peculiar velocities are simply related to density perturbations via the continuity equation

$$\nabla \cdot \vec{v}(\vec{x}, a) \equiv \theta(\vec{x}, a) = -a^2 H(a) \frac{\mathrm{d}\delta(\vec{x}, a)}{\mathrm{d}a} = -aH(a) f(a) \delta(\vec{x}, a) \tag{1.16}$$

where θ is the velocity divergence, a convenient scalar field describing velocities. In Fourier space, the velocity field is simply proportional to the density. The velocity divergence power spectrum $P_{\theta\theta}$ is an important ingredient for models of redshift-space distortions, as we discuss in the following section.

1.4.4 The amplitude of the power spectrum

The matter power spectrum $P(k)$ represents the variance of density perturbations at a given wavenumber k. The total variance of the density field is therefore the sum of all contributions over all available three dimensional modes. This is equivalent to the correlation function at zero separation:

$$\sigma^2 = \xi(r=0) = \frac{1}{(2\pi)^3} \int \mathrm{d}^3k\, P(k) = \frac{1}{2\pi^2} \int_0^\infty \mathrm{d}k\, k^2 P(k), \tag{1.17}$$

which diverges if we use the linear prediction for the matter power spectrum. This is because the linear power spectrum is the evolution of a nearly scale invariant power spectrum, equivalent to white noise, so the variance simply keeps increasing as we consider larger ranges of scales. Therefore, it is convenient to smooth the linear density field using a three-dimensional top-hat filter with radius R. The variance of the smoothed field is then

$$\sigma_R^2 = \frac{1}{2\pi^2}\int_0^\infty \mathrm{d}k\, k^2 P(k) W_R^2(k), \tag{1.18}$$

where $W_R(k) = 3[\sin(kR) - kR\cos(kR)]/(kR)^3$ is the Fourier transform of the top-hat filter.

In studies of large-scales structures, it is common to use σ_R as a parameter defining the amplitude of the linear power spectrum. As discussed before, this amplitude depends on the values of A_s (Eq. 1.13) and h (which determines the age of the Universe and how long structures could have grown). Therefore σ_R is degenerate with A_s and h though is more representative of the amplitude of $P(k)$ at later times. Other energy density parameters Ω_x also affect this amplitude, but these also change the overall shape and are not degenerate with σ_R.

The variance σ_R is a decreasing function of R. Historically, the chosen values for R give variances near unity, which correspond to the regime where linear theory should break. Recently, the value of $R = 8h^{-1}$Mpc has been used in several analysis, though it has been argued that chosing $R = 12$ Mpc (without the h dependency) is a better choice to break degeneracies (Sánchez 2020).

In measurements of redshift-space distortions and peculiar velocities, there is a degeneracy between the value of f and the amplitude of the power spectrum, σ_8. Therefore, measurements can only constrain the combination $f\sigma_8$.

1.5 Cosmological probes of expansion

In this section, I present the basics of the cosmological observables that allow us to learn about dark-energy. Some of these are mostly sensitive to the background evolution presented in section 1.3, while others depend on the matter perturbations and their statistical properties as discussed in section 1.4.

1.5.1 Direct measurements of H_0

The Hubble constant H_0 is probably one of the first cosmological parameters to be estimated by the one giving its name (Hubble 1929). Today, there are a few techniques to estimate H_0 which yield roughly independent results. See Riess 2020 for a quick review of the latest results.

The most traditional method is known as the *distance ladder*. The idea is to measure the distance-redshift relationship of objects well in the Hubble flow. The distance to the closest objects in the Solar neighbourhood can be estimated with the parallax method. The Gaia satellite has the current largest catalogue of parallax measurements, of more than a billion stars. Parallax is one of the few direct distance estimating methods. They can be used to measure the intrinsic luminosity of some objects thought to be standard candles, such as Cepheid stars, RR Lyrae, and the largest red giant stars. Distances to farther objects can be estimated using these candles. They can also be used to calibrate other brighter standard candles, such as type-Ia supernovae, which can be observed at the largest distances. Riess, Casertano, et al. 2021 contains the latest measurements using Gaia parallaxes, Cepheids and type-Ia supernovae to determine $H_0 = 73.0 \pm 1.4$ km/s/Mpc. Freedman et al. 2019 is latest measurement of distances using the tip of the red giant branch.

The distance to the galaxy NGC 4258 could be determined thanks to the presence of a water maser orbiting the center of this galaxy. The proper motions of several clouds orbiting close to the central massive black hole could be measured both in radial and angular directions, strongly constraining the dynamics of the system (Herrnstein et al. 1999). The most recent measurement yields $D = 7.576 \pm 0.082$ (stat.) ± 0.076 (sys.) Mpc (M. J. Reid et al. 2019), which can be used as an alternative to Cepheids to anchor the distance ladder and provide an estimate to H_0.

Another alternative method is based on the time-delay of the signals emitted from a quasar behind a strong gravitational lens. The lens creates multiple images of the same background quasar, but the light paths have slightly different lengths. Since quasars are variable objects, the same variability is observed with a delay of several days between the different images. By modelling the distribution of matter between the quasar and us, it is possible to convert these time delays into an estimate of H_0. The "H_0 Lenses in COSMOGRAIL's Wellspring", or H0LiCOW, collaboration produced the latest comprehensive measurement of H_0 using strongly-lensed quasars (Wong et al. 2019). An alternative measurement has been performed using strong lenses from the Sloan (SLACS). They are compared to H0LiCOW in Birrer et al. 2020.

More recently, gravitational waves from a merger of two black holes were observed for the first time by the LIGO collaboration (T. L. S. Collaboration and the Virgo Collaboration 2016). Not long after, a merger of two neutron stars was observed by both LIGO and Virgo, but this time an electromagnetic counterpart was also detected (T. L. S. Collaboration and T. V. Collaboration 2017), pointing to the galaxy where the event occurred. Given the well predicted shape of the wave form and its dependency on the masses of the neutron stars, it was possible to estimate the distance to the host galaxy. Combining with a measurement of its redshift, a single event could provide an estimate of H_0 (Abbott et al. 2017). This opened the field of cosmology using standard sirens, i.e., gravitational wave sources.

The cosmic microwave background can yield an estimate of H_0 but it is strongly degenerate with other unknown parameters, such as curvature or dark-energy densities. Some of these degeneracies are reduced when considering the effect of gravitational lensing of the CMB or when combining with other probes of late times. Therefore, precise measurements of H_0 from the CMB alone are only possible when considering more restrictive models, such as a flat space with a cosmological constant.

1.5.2 Type-Ia supernovae

As mentioned earlier, type-Ia supernovae (SNIa) can be used as standard candles for absolute distance measurements, if they are anchored by another method. The SNIa can also be used alone to produce relative distance measurements and constrain dark-energy. In this case, no anchor is required and the only assumption is that the SNIa intrinsic brightness does not evolve with redshift.

The main observable are the fluxes of SNIa as a function of time in different photometric bands, known as light-curves. Spectroscopic follow up observations of the explosion can confirm the type of the supernova based on the features present in their spectra. Another key ingredient is the redshift of the host galaxy of the SNIa, which is commonly measured with spectroscopy as well.

Spectro-photometric models of SNIa are used to fit the observed light-curves, yielding their apparent magnitudes at peak luminosity in a given photometric band. These models account for correlations between color and duration of light curves and the peak magnitude, reducing the intrinsic scatter in these magnitudes from 40% to roughly 15%. It is essential to obtain accurate and precise measurements of SNIa fluxes in order to obtain the best cosmological constraints. Large sets of realistic simulations of the data are required in order to correct for selection effects. The final product of the analysis is a set of distance moduli (Eq. 1.6) and their host-galaxy redshift, which can then be compared to models of expansion of the Universe.

Distance moduli depend on dark-energy through the integral of $H^{-1}(z)$. In order to obtain good constraints on dark-energy properties, it is important to have a large redshift coverage, at least covering the transition between matter-dominated to dark-energy-dominated eras, so $0 < z < 1$. The advantage of SNIa for dark-energy studies is that they can span these redshifts with a high sampling rate, which helps in the study of the expansion-rate. One of the inconveniences is that SNIa are complex and poorly understood astrophysical events, the intrinsic scatter in luminosity cannot be reduced to better than 12%, potentially limiting the gains constraining power from future experiments.

The latest comprehensive study of SNIa combines data from more than a dozen projects into a single sample, the Pantheon sample, from which dark-energy constraints were derived (D. M. Scolnic et al. 2018). The Dark Energy Survey also measured a more recent sample of few hundreds of SNe (Brout, Sako, et al. 2019; Brout, D. Scolnic, et al. 2019; Kessler et al. 2019), but not all of them have spectroscopic confirmation that they are of type Ia. Their constraints on dark-energy are not yet competitive compared to the Panthon sample. The Zwicky Transient Facility (ZTF, Graham et al. 2019) is currently observing the Northern sky on a search for transient events and is expected to discover around 5000 spectroscopically confirmed SNIa at low redshifts ($0 < z < 0.12$) until 2023. After 2023, the Rubin Observatory Legacy Survey of Space and Time (LSST) will take over in the Southern hemisphere and will discover more than 300 thousand SNIa up to $z < 0.5$.

While ZTF and Rubin's samples of SNIa will not decrease significantly the errors on dark-energy parameters, they cover a redshift range where other powerful probes, such as BAO or weak-lensing, lack of statistical power. Furthermore, at lower redshifts when dark-energy is dominant, SNIa are complementary to redshift-space distortions (RSD) when it comes to testing the validity of General Relativity or constraining altenate models of gravity, as solutions for dark-energy.

Not only SNIa are a great probe of the expansion history, they can also provide peculiar velocities of their host galaxies via their inferred distances. These peculiar velocities and their statistical properties can complement RSD analysis when measuring the growth-rate of structures (Eq. 1.15). Estimates of $H(z)$ and $f(z)$ can help break degeneracies between simple dark-energy models and more involved models of gravity (Kim et al. 2020; Graziani et al. 2020). Chapter 5 is dedicated to this topic, to which I plan to dedicate the future years of my research.

1.5.3 Big Bang nucleosynthesis

In the post-inflation Universe, when temperatures are below the equivalent of 100 MeV, perturbations in the matter and radiation fields are quite small and most of the physics is dictated by the interactions between protons, electrons, neutrons, and photons, as described by the Boltzmann equations. As the Universe cools down and rarefies, protons and neutrons start forming atoms of deuterium, tritium, helium and heavier elements. This process is known as the Big Bang nucleosynthesis (BBN).

The relative amount of each of the formed elements depends on the expansion rate of the Universe at that time as well as the physical density of baryons $\omega_b = \Omega_b h^2$ and radiation $\omega_r = \Omega_r h^2$. Given that the energies involved are within reach of particle accelerators, these reactions can be studied with great detail on Earth, allowing us to build accurate models of the BBN (see Pitrou et al. 2021 for the latest calculations and references therein).

Observations of the primordial abundances can be compared to the predictions by BBN models. Abundances of deuterium, helium, and others can be estimated from spectroscopic observations of HII regions in metal-poor galaxies or from absorption lines of the intergalactic medium in quasar spectra. The most up-to-date measurements of the primordial helium-4 abundance yields $Y_p = 0.2453 \pm 0.0034$ (Aver et al. 2021), while the deuterium one is $\mathrm{D/H} = (2.527 \pm 0.030) \times 10^{-5}$ (Pitrou et al. 2021). While observations are consistent with BBN models for deuterium and helium, the abundance of lithum-7 exhibits a factor 3 discrepancy, which is a huge problem in BBN but quite often neglected.

The temperature fluctuations in the cosmic microwave background (CMB) are also very sensitive to the physical baryon density ω_b. Historically, the values obtained from CMB have been in good agreement with BBN measurements, showing that baryons make up to around 16% of the total matter content of the Universe, or $\omega_b = (2.195 \pm 0.022) \times 10^{-2}$. The agreement between two quite independent probes is one of the great successes of the current cosmological model, thought they also enforce the need for a dark-matter component.

1.5.4 Baryon acoustic oscillations

Baryon acoustic oscillations (BAO) is the name given to the propagation of sound waves in the primordial plasma (baryons and photons), prior to recombination. Because of the high pressure on small scales at those times, each initial density perturbation had a spherical density wave around them propagating outwards at the speed of sound in that medium. The speed of sound in the plasma is given by

$$c_s(z) \equiv \sqrt{\frac{1}{3[1 + R(z)]}} \tag{1.19}$$

where $R(z) = 3\rho_b/4\rho_\gamma$ is the baryon-to-photon ratio. The propagation of sound waves occurred until the temperatures and densities dropped to values such that baryons no longer felt the pressure from photons, known as the *drag epoch*, which is close in time to the recombination (but technically not the same eopch). This process left a slight overdense shell around each initial perturbation with a radius given by

$$r_{\mathrm{drag}} \equiv r_s(z_{\mathrm{drag}}) = \int_{\infty}^{z_{\mathrm{drag}}} \mathrm{d}z' \, \frac{c_s(z')}{H(z')} \tag{1.20}$$

which is known as the *sound horizon at drag epoch*, or the BAO scale. Today, r_d has a physical size of about 147 Mpc, much larger than any collapsed structure in the Universe. As one can see from Eqs. 1.19 and 1.20, r_{drag} mainly depends on ω_b and ω_c assuming the CMB gives a precise estimate of ω_γ. The dependency of r_{drag} is mainly through ω_b, which is useful when constraining dark energy models for instance.

After recombination, the sound horizon scale only increases in size due to the expansion, or equivalently, its comoving size remains unchanged. Therefore, the BAO scale is a great *standard ruler* to study the expansion rate of the Universe. In practice, the BAO scale is observed statistically in the two-point function of the matter density field, so it is often classified as an statistical standard ruler. In configuration space, the correlation function $\xi(r)$ presents a small peak at separations corresponding to the BAO scale r_d, while in Fourier space the power spectrum $P(k)$ contains an oscillatory pattern as a function of scale with a period proportional to the BAO scale. In Chapters 3 and 4, I present my past work in the measurement of the BAO scale using Lyα forests and galaxies, respectively, as tracers of the matter density field.

Given that a galaxy survey is made of angular positions and redshifts, which are true observables, the BAO peak is effectively measured as an angle $\Delta\theta_{\mathrm{BAO}}$ or as a difference in redshift Δz_{BAO}. These can be modelled as ratios of distances to the BAO scale r_d as

$$\Delta\theta_{\mathrm{BAO}}(z_{\mathrm{eff}}) = \frac{D_M(z_{\mathrm{eff}})}{r_d} \tag{1.21}$$

$$\Delta z_{\mathrm{BAO}}(z_{\mathrm{eff}}) = \frac{D_H(z_{\mathrm{eff}})}{r_d} \tag{1.22}$$

where z_{eff} is the effective redshift of the galaxy survey, D_M is the comoving angular diameter distance (Eq. 1.4), and D_H is the Hubble distance (Eq. 1.2).

There are two ways BAO can be used to constrain cosmological models, depending if we assume that r_{drag} is known or not. If r_{drag} is known, i.e. given by Eq. 1.20 using some value for ω_b (given by the CMB or BBN for instance), then BAO measurements are converted to absolute distance measurements which depend only on $H(z)$. Therefore, BAO can constrain H_0, curvature and dark energy. If r_{drag} is supposed to be unknown but still a standard ruler, then BAO constraints the ratio of $E(z) = H(z)/H_0$ to the combination $H_0 r_{\mathrm{drag}}$ which is now degenerate. This is similar to type Ia supernovae, where their absolute magnitude is degenerate with H_0. By combining several BAO measurements at different effective redshifts, BAO is a powerful probe of dark energy and curvature.

Current BAO measurements span effective redshifts from 0.1 to 2.3. The Sloan Digital Sky Survey (SDSS, Eisenstein, Weinberg, et al. 2011; Blanton, Bershady, et al. 2017) has measured more than 2 million redshifts spectroscopically in the past twenty years, producing the largest maps to date of the distribution of matter in the Universe. In addition to SDSS, surveys such as FastSound (Okumura et al. 2016), Vipers (Pezzotta et al. 2017), 6 degree field galaxy survey (6dFGS, Beutler et al. 2012) and WiggleZ (Parkinson et al. 2012) also produced BAO measurements using galaxies, though the volumes probed and the number of galaxies is inferior to SDSS. The latest cosmological constraints from BAO are described in Alam, Aubert, et al. 2021.

1.5.5 The cosmic microwave background

The cosmic microwave background (CMB) is one of the richest cosmological probes of all. The photons we receive today last scattered on baryons at a redshift of about 1100, corresponding to roughly 380 000 years after the Big Bang. It is the oldest information that we can measure from the Universe today.

The average temperature $T_{\mathrm{CMB}} = 2.72548 \pm 0.00057$ K (Mather et al. 1994; Fixsen 2009) of these photons, measured the last time by the COBE satellite, tell us on how much energy density from radiation there is in the Universe. From the black body Bose-Einstein distribution of photons, we have

$$\rho_\gamma = \frac{\pi^2 k^4}{15\hbar^3 c^3} T_{\mathrm{CMB}}^4 \tag{1.23}$$

The fluctuations around this average temperature, ΔT, and the polarisation of these photons trace the structures back at the recombination epoch. Given its early-times nature, the temperature and polarisation fields are extremely well described by Gaussian statistics. Most of the information is therefore contained in the two point functions of these fields. Given that these fields are two dimensional, functions of the position angle in the sky (θ, ϕ), it is convenient to decompose these fields into a basis of spherical harmonic functions $Y_{\ell m}(\theta, \phi)$, which amplitudes are denoted $a_{\ell m}$. The angular power spectrum is simply the variance of these amplitudes: $C_\ell = \langle a_{\ell m} a^*_{\ell m}\rangle$, which in linear theory is simply a function of ℓ and independent of m. The temperature and both polarisation modes (E and B) can be decomposed into spherical harmonics, so we can estimate all cross power spectra, e.g., $C_\ell^{TE} = \langle a^T_{\ell m} a^{E*}_{\ell m}\rangle$ is the cross temperature and E-mode polarisation power spectrum.

The temperature and polarisation auto and cross power spectra are exquisitely well modelled by linear perturbation theory. In the most basic ΛCDM model, the power spectrum is a function of only six parameters: the angular scale of baryon acoustic oscillations θ_*, the physical density of baryons ω_b and dark-matter ω_c, the primordial power spectrum amplitude A_s and slope n_s, and the optical depth τ. The fact that such a model with so few free parameters can describe so well the observations is one of the greatest achievements in modern physics. A great description of the CMB physics from first principles can be found in Dodelson et al. 2020. Several codes are available to compute models for the CMB such as CAMB[3] (Lewis et al. 2000) and CLASS[4] (Lesgourgues 2011).

Explain how the power spectrum depends on the parameters

Latest measurements: Planck satellite (Planck Collaboration et al. 2020), Atacama Cosmology Telescope (ACT, Aiola et al. 2020), South Pole Telescope (SPT, Aylor et al. 2017; Balkenhol et al. 2021; Dutcher et al. 2021), BICEP/Keck (BICEP/Keck et al. 2021) for B-modes.

1.5.6 Redshift-space distortions

Matter is not static in the Universe. Due to gravity, matter flows from underdense regions towards overdense ones. These velocities are commonly called *peculiar velocities.* The radial component of peculiar velocities alters the observed redshift of an object, due to the Doppler effect. Therefore, the total observed redshift $z_{\rm obs}$ is a combination of its cosmological redshift $z_{\rm cos}$, due to the expansion of the Universe, and the peculiar redshift $z_{\rm pec}$, due to the Doppler effect:

$$1 + z_{\rm obs} = (1 + z_{\rm cos})(1 + z_{\rm pec}) \tag{1.24}$$

where

$$z_{\rm pec} = \sqrt{\frac{1 + \frac{\vec{v}\cdot\hat{n}}{c}}{1 - \frac{\vec{v}\cdot\hat{n}}{c}}} - 1 \approx \frac{\vec{v}\cdot\hat{n}}{c} \tag{1.25}$$

The first equality is the definition of the relativistic Doppler effect, $\vec{v}$ is the velocity and $\hat{n}$ is the radial unitary vector. The right-hand side is the non-relativistic approximation, which is accurate for typical velocities of matter flows in our Universe.

When converting observed redshifts into comoving distances, peculiar velocities introduce a small error such that

$$s(z_{\rm obs}) \approx r(z_{cos}) + \frac{(1 + z_{\rm cos})}{H(z_{\rm cos})}\vec{v}\cdot\hat{n}, \tag{1.26}$$

where s is the *redshift-space* distance and r is the *real-space* distance. The errors caused by

[3] https://camb.info/

[4] https://lesgourg.github.io/class_public/class.html

peculiar velocities distort the observed distribution of matter/galaxies since we cannot in general decouple the velocities and the Hubble flow. This effect is observable and named *redshift-space distortions* (RSD). RSD are a powerful probe of the dynamics of the matter field, i.e., on how velocities are related to the densities, and how they contribute to the growth of structures over time. More generally, observations of RSD can be used to test the validity of general relativity since it is a probe of the strength of gravity.

The density contrast of matter is modified when observed in redshift-space relative to real-space, given the redshift-space distortions. Mass conservation implies that

$$[1+\delta_s(\vec{s})]\mathrm{d}^3 s = [1+\delta(\vec{x})]\mathrm{d}^3 x, \tag{1.27}$$

such that in Fourier space we obtain, in the linear regime (Kaiser 1987)

$$\delta_s(\vec{k}) = (1+f\mu^2)\delta(\vec{k}) \tag{1.28}$$

where f is the growth-rate of structures defined in Eq. 1.15 and $\mu = \vec{k}\cdot\hat{n}/k$ or the cosine of the angle between the wavevector and the line of sight. The power spectrum in redshift-space assuming linear perturbations is simply

$$P_s(k,\mu) = (1+f\mu^2)^2 P_m^{\mathrm{lin}}(k) \tag{1.29}$$

This means that the redshift-space matter power spectrum has radial modes enhanced by a factor of $(1+f)^2$ (where $f \sim 1$) relative to modes transverse to the line of sight. This enhancement is observable with galaxy surveys. If the normalisation of the linear matter power spectrum is parametrised by σ_8 (Eq. 1.18), then the actual measured quantity is the product $f\sigma_8$. Transposed to a given effective redshift z_{eff} of a galaxy survey, we need to scale σ_8, which is usually defined at $z=0$, using the growth factor $D(z)$, such that the measured quantity is $f(z)\sigma_8 D(z)$.

The observable $f(z)\sigma_8 D(z)$ is mostly sensitive to the amount of dark matter ω_m, which drives the growth of structures, and $H(z)$, which damps the growth (see Eq. 1.14). Therefore, it can be used to constrain dark energy models. More generally, measurements of $f(z)\sigma_8 D(z)$ can be used to test the the validity of general relativity on large scales, which is the commonly assumed theory of gravity.

The latest most relevant measurements were performed using data from the Sloan Digital Sky Survey (SDSS), including

- the SDSS Main Galaxy Sample Howlett et al. 2015,
- the Baryon Oscillation Spectroscopic Survey (BOSS, Alam, Ata, et al. 2017),
- the extended BOSS luminous red galaxy sample (eBOSS LRG, Julian E Bautista et al. 2020; Gil-Marín et al. 2020),
- the eBOSS emission line galaxy sample (eBOSS ELG, Tamone et al. 2020; de Mattia et al. 2021),
- the eBOSS quasar sample (eBOSS QSO, Hou et al. 2021; Neveux et al. 2020),

In chapter 4 I present my contributions to the measurement of the growth-rate of structures using the eBOSS LRG sample (Julian E Bautista et al. 2020). The cosmological implications of SDSS growth-rate measurements are described in Alam, Aubert, et al. 2021.

1.5.7 Weak gravitational lensing

Photons follow space-time geodesics. Space-time is distorted in the presence of a source of gravitational potential, which is typically in the form of a mass concentration. Therefore, the matter distribution in the Universe bends photon trajectories from distant sources. This phenomenon receives the name of *gravitational lensing*, since the theory describing light propagation on a gravitational field is analogous to classical optics. Gravitational lensing is a rich cosmological probe since the distorion of photon trajectories depends on both the baryonic and dark matter. From lensing measurements we can learn about the total matter distribution in an expanding Universe.

In the case of an extended source of photons, e.g., a galaxy, light from different angular positions within the source take slighly different paths towards the observer. If this extended source is placed in the background of a mass concentration - the lens - each path will suffer a slightly different bending, which depends on the impact parameter of each photon relative to the center of this lens. Also, due to conservation of surface brightness (is this the correct name?), the total flux is also increased. The final result is an image shifted, distorted and brighter.

Lensing measurements use shifts, distortions and increase in flux to determine properties of the lenses. These measurements are hard since we do not have access to the original unlensed position, shape and flux of a given galaxy. One remarkable exception is lensing in its strong regime. When the ratio between impact parameter of the source and mass of the lens is below some threshold - the Einstein radius - multiple images of the same source are created. Strong lensing allows us to estimate the mass and density profile of a given lens. Moreover, if the source is variable in time, this variability is slightly delayed between each of the multiple images, which allows us to constrain the expansion of the Universe. As mentioned in section 1.5.1, strongly lensed quasars (variable sources) are used to constrain H_0, under the assumption that we can properly model the lens density profile.

However, statistical measurements of lensing, such as correlations with overdensities, can be performed by making assumptions on the statistical properties of the unlensed sample of galaxies.

weak regime we measure shapes and correlate themselves (shear-shear) or with the galaxy field (galaxy-shear)

Sensitive to: the amplitude of the shear power spectrum, $S_8 = \sigma_8\sqrt{\Omega_m/0.3}$.

Latest measurements: Kilo Degree Survey (KiDS, Heymans et al. 2021), Dark Energy Survey Year 3 (DES-Y3, D. Collaboration et al. 2021), Hyper Supreme Cam first year (HSC, Hikage et al. 2019)

2 Observing the Universe with spectroscopy

Contents

2.1 Selecting the objects to observe . . . 24
2.2 Pointing fibres to the sky . . . 25
2.3 From electrons to spectra . . . 26
2.4 From spectra to redshifts . . . 28
2.5 From redshifts to cosmology . . . 28

In the last two decades, spectroscopy became one of the most powerful techniques to survey the galaxies of our Universe. Particularly thanks to its capability to obtain precise galaxy redshifts, spectroscopy allows us to build precise maps of the distribution of matter in three dimensions.

This chapter is an overview on how to observe galaxies with spectroscopy and how the data is treated from the target selection all the way to the redshifts. I expose my work on improving the spectroscopic data reduction pipeline for the extended Baryon Oscillation Spectroscopic Survey (eBOSS), for which I was the *Lead Data Scientist* for 3 years.

Naturally, this chapter will focus on the spectroscopic observations with the Sloan Digital Sky Survey (SDSS), but the majority of the concepts introduced here also apply to the Dark Energy Spectroscopic Instrument (DESI).

2.1 Selecting the objects to observe

The first step to build a spectroscopic survey is to pre-select objects to be observed. This step, known as *target selection*, is required since you need to know where to point the optical fibers that take the light from an object to the spectrograph. Therefore, we cannot simply observe all objects in a given field, we need to choose which targets to observe.

For the target selection, a prior *photometric or imaging* survey is required. In the first years of SDSS, a photometric survey was carried out, covering more than XXX deg^2 of the sky York et al. 2000. The focal plane was equiped with six rows of five charge-coupled devices (CCD), each one covered with one of the SDSS filters: u, g, r, i or z J. E. Gunn et al. 1998; Doi et al. 2010. A technique named drift-scanning was used to continuously observe "stripes" of constant declination during the night. SDSS was the first of its kind to produce a systematic survey of the Universe in the optical domain.

Images were reduced using the SDSS photometric pipeline Lupton et al. 2001; Padmanabhan et al. 2008. Fluxes/magnitudes and their uncertainties were computed for each detected object in five colour bands. Based on their fluxes and angular sizes relative to the point-spread function (PSF), each object received a photometric classification as star or galaxy.

The final list of objects with their respective fluxes and angular positions is the input for targeting algorithms. These algorithms aim to select a given type of object for spectroscopic follow-up, based solely on their fluxes and colors. For galaxy surveys, it is vital to be able to

Table 2.1: Surveys and their target selection algorithms

Sample	Redshift range	Reference
SDSS Main Galaxy Sample	$0.0 < z < 0.2$	Strauss et al. 2002
BOSS LOWZ galaxies	$0.2 < z < 0.4$	B. Reid et al. 2016
BOSS CMASS galaxies	$0.4 < z < 0.7$	B. Reid et al. 2016
BOSS Lyα forest quasars	$2.0 < z < 3.5$	Ross et al. 2012
eBOSS LRGs	$0.6 < z < 1.0$	Prakash et al. 2016
eBOSS ELGs	$0.7 < z < 1.1$	Raichoor et al. 2017
eBOSS quasars as tracers	$0.8 < z < 2.2$	Myers et al. 2015
eBOSS Lyα quasars	$2.0 < z < 3.5$	Myers et al. 2015 N. Palanque-Delabrouille et al. 2016

distinguish between galaxies - the objects of our interest - and stars - which belong to our own galaxy and have a distinct scientific purpose. Additional colour cuts also help selecting a given redshift range for particular types of galaxies.

Since we are interested in the clustering of galaxies, it is essential to obtain a relatively homogeneous angular density of targets so to avoid spurious correlations. Target selection algorithms enforce a requirement of about 15 per cent angular fluctuations on the number density of targets. Residual fluctuations have to be corrected before any clustering measurements, I will discuss about this in section 2.5.

Table 2.1 provides a summary of target selection algorithms for several types of galaxy types and redshift ranges. (see `https://www.sdss.org/science/technical_publications`)

2.2 Pointing fibres to the sky

Once the targets are chosen, we need to define the observing strategy for spectroscopy. This strategy is defined based on several constraints, such as

- the focal plane dimensions, which is a one meter diameter plate holding 1000 optical fibers;
- the field of view of the telescope, which is about 5 deg^2 for the plates;
- the number of fibers. There are a total of 1000 fibers available of which 80 are used for sky observations and 20 for standard stars;
- the size of the footprint, which is roughly 10 000 deg^2;
- the fiber completeness, i.e., the fraction of targets receiving an optical fiber. The completeness has to be usually above a certain threshold over all the footprint;
- exposure times and total observing time available. Exposure times are dependent on the average signal-to-noise ratio of the observed targets, which should reach a certain threshold. The total observing time of the program is roughly four to five years.
- visibility window of a given patch of the sky at a given time of the year;
- priority for fiber assignement. Some types of targets have higher priority than others, which affects the fiber completeness of the low-priority samples.

The process of dividing the sky into overlapping projections of the focal plane is called *tiling*. A detailed description of the tiling algorithm can be found in Blanton, Lin, et al. 2003. Once the tiling and fiber assignement are set, this information is sent to the plate production and drilling of holes that will hold the optical fibers. Focal plane plates are drilled a few months before observing and are unique for a particular patch of the sky and observing time. Not observing the plate at the designed times causes loss of flux due to different refraction caused by the atmosphere.

The drilled plates are sent to the Apache Point Observatory (APO) in New Mexico where the Sloan 2.5-meter Telescope is based. On the mountain, observers attach the plates into cartriges that will fit at the focal plane of the telescope. There are about 15 cartriges, each equiped with 1000 optical fibers. The fibers are plugged by hand, by one or two observers during the afternoon preceding the observation night. Plates are unplugged from their cartrige once a large enough number of exposures has been taken. A minimum of 3 exposures are taken per plate.

The light of the objects is transported by the optical fibers through the Sloan spectrographs. There are two spectrographs attached at the focal plane of the telescope. Each spectrograph receives the light from 500 fibers and passes it through a beamsplitter, dividing it into a red and blue channels. Each channel has is own grism that spreads the light over wavelength before hitting the CCDs. The blue camera observes roughly from 3500 to 6000 Å and the red camera from 6000 to 10500 Å. The resolution $R \equiv \lambda/\Delta\lambda$ increases with wavelength from 1500 to 2000 on the blue camera and from 2000 to 2500 on the red camera.

In addition to the science exposures (observing galaxies), a small set of calibration exposures is also taken, typically at the beginning and at the end of the observing run. Flat exposures are taken with lamps that emit over all wavelengths. The light is passed through the spectrographs, so we refer to these as fiber-flats, as opposed to the exposures taken without the spectrographs, named super-flats. With another type of lamp, which emit narrow lines at some specific wavelengths, arc exposures are obtained, that are used to derive the wavelength-pixel relation.

2.3 From electrons to spectra

This section describes the data reduction pipeline of spectroscopic observations by the SDSS telescope, for which I contributed as the eBOSS Lead Data Scientist. This automated pipeline transforms the counts stored in CCDs into calibrated spectra, for which redshifts are estimated. The software, named `idlspec2d`, was written in Interactive Data Language (IDL) and can be found online[1]. The latest version used in Data Release 16 of eBOSS data is `v5_13_0` (Ahumada et al. 2020).

The dispersed light of each object falls onto CCD detectors containing 2048x2048 square 24μm pixels. There are 500 traces per CCD, except when fibers are broken or unplugged by accident. The traces of each spectra are parallel and slighly curved towards the edges. They are separated by about 7 pixels.

The first step of the data reduction is to remove bias and dark, mask cosmic rays and other known bad pixels, convert counts into electrons using estimated gain values, and correct for the super-flat image (flat taken without the spectrograph).

The next step is to extract the total number of counts per wavelength and per object. One of the axis of the CCD is aligned with the wavelengths, but we do not know the wavelength

[1] https://svn.sdss.org/public/repo/eboss/idlspec2d/tags/v5_13_0/

solution at this point. The other axis is aligned with fiber number. The extraction of the fluxes is performed by bundles of 20 fibers. A set of 20 Gaussian profiles plus a third order polynomial term are fit simultaneously over the counts. From the best-fit parameters of the Gaussian, one can compute the total flux at each wavelength for each object. This fit is performed regardless of whether the fibers contain flux from sky, stars or galaxies. The extraction is performed similarly to science, flat and arc exposures.

One important aspect of extraction is: what do we use as weights in the fit? For SDSS-II and III, the extraction used the total estimated variance of each pixel, assumed to be Poisson with mean equal to the number of observed hits in the pixel. However, in SDSS-IV eBOSS we pushed the limits of the instrument by observing fainter objects. In this regime, we started to observe biases due to this weighting scheme in the extraction. The ideal extraction would use the true variance (Horne 1986), not the estimated one, as a weight. Using the estimated one yields a bias in the final fluxes. We modified the extraction algorithm such that it would use a flux-independent weight for fit, yielding unbiased fluxes. The price to pay is that this extraction is less optimal, yielding slighly larger flux uncertainties. Biased fluxes affected particularly the analysis of Lyα forests, as described in Chapter 3 or in the appendix of Julian E. Bautista et al. 2017.

The fiber-flat images are used to calculate the traces positions and widths (more precisely than in science images) and to correct for throughput variations accross fibers. The arc images are used to calculate the wavelength solution and the dispersion in the wwavelength direction based on the line widths. Sky lines in science exposures are eventually used to do small adjustments to the arc-image solution.

The flux in the sky fibers are used to fit a sky model in units of counts. A polynomial dependency over fiber index is used to account to variations over the focal planne. This sky model is then subtracted from all science spectra, including the sky spectra themselves and calibration stars. The sky-subtracted sky fibers are a good metric to evaluate the quality of sky subtraction algorithm.

The next step of the reduction is the *flux calibration*, which converts the observed counts into flux in physical units. The spectra of standard stars are the main ingredient of the flux calibration. The stars chosen for calibration are of type F, with small variations in temperature and metallicity. Physical models of their spectral emission can be obtained through complex stellar synthesis calculations, including all absorption features. The goal is to fit absorption lines to the data in order to determine the exact model for each observed star. We start by isolating the absorption lines in the observed spectrum (in units of counts) by fitting a smooth function over its shape, then dividing the whole spectrum by this model. The same is done for the physical stellar models, so the fit only uses the absorption lines information. Once the best parameters of the star are found, a calibration vector is constructed by simply taking the ratio of the observed counts to the full model including its smooth shape. A set of ten stars are fit independently and a single calibration vector is obtained from them. This final calibration vector is then applied to all other galaxy spectra in order to convert their flux into physical units. During the last years of eBOSS, I updated the set of physical stellar models from the Kurucz model to those used in DESI (ref? Allende-Prieto?) which have a larger diversity in stellar parameters and more precise absorption features. This update contributed to a significant reduction of flux calibration residuals (add Figure??) computed using stacks of spectral regions of quasars without emission or absorption lines.

Once individual science exposures are converted into physical flux units, we proceed to the coaddition of these exposures into a single set of spectra. For a given object, a B-spline is fitted over all observed spectra, using a new wavelength grid with constant steps in $\log_{10}\lambda$ of 10^{-4}. The best-fit spline is the final coadded spectrum for this object. The coaddition is made independently for each object. At this stage, we also combine spectra from blue and red cameras into one single spectrum covering the full wavelength range of 3500 to 10500 Å. The last step of this process is the calculation of potential broadband distortions in flux caused by atmospheric differential refraction (ADR). Using information from the plate design, the position of the fibers in the plate and the actual observations (airmass, hour-angle), one can compute a correction vector that is also applied to all spectra.

During the whole reduction, pixels or whole fibers can be masked due to any issues, or when the robustness of flux calculations is compromised. Each pixel has a flux and an uncertainty estimates, the latter is expressed as an inverse variance, which can be used directly as a weight in scientific analyses.

This concludes the so-called two-dimensional reductions, that convert 2D CCD images into a set of calibrated coadded sky-subtracted 1D spectra.

2.4 From spectra to redshifts

The next and last step of the automated data reduction pipeline is the spectral classification and redshift measurement. A set of physical templates of stars, galaxies and quasars is fit to each spectrum by a simple χ^2 minimization. For each template, we scan over several values of redshifts to obtain the minimum χ^2. The redshift ranges probed depend on the type of template: stars are at $z = 0$ with allowed peculiar velocities, galaxies are in $0 < z < 2$ and quasars in $0 < z < 7$. The five pairs of template-redshift producing the smaller χ^2 values are stored. Redshift uncertainties are estimated using the χ^2 profiles around the minima. If the difference between the first and second best-fit χ^2 values is smaller than a certain threshold (corresponding to roughly 5σ for one parameter), a warning flag is set, meaning that the classification is not to be trusted.

A program of visual inspection of reduced spectra, with their automated classification and redshift estimates, is carried out following the first observations of a new survey. Visual inspection is a important step in order to verify the quality of the data reduction and the classification process. A truth table containing the visually confirmed redshifts and classifications for thousands of spectra is one of the results of the visual inspection. This truth table is used to compute the actual density of tracers that are obtained for a given target selection, as a function of redshift. Spectral features caused by problems in the reduction were then reported to the pipeline team.

During the first months of eBOSS, I coordinated a program of visual inspection where about 15 members analysed about a thousand spectra each (with some overlap for cross-checking results). This provided a truth table for the Luminous Red Galaxies from eBOSS. Similar programs were carried out for the eBOSS Emission Line Galaxies and quasars. The inspections of eBOSS quasars continued throgh the whole program, where a small fraction of the spectra without confident automated classifications were inspected. In DESI, a larger visual inspection program was put in place for the same goals.

2.5 From redshifts to cosmology

Description of catalog generation. Shall this go on the clustering part ?

3 The high-redshift Universe and its forests

Contents

3.1 Forests as a tracer of the Universe's structures 29
3.2 Baryon acoustic oscillations in the forests 31
3.2.1 Transmission field 32
3.2.2 Two-point correlation functions 33
3.2.3 Correction matrices 34
3.2.4 BAO model 34
3.3 Impact of redshift errors 34
3.4 Weak-lensing of forests 34

Until today, the Lyα forest in quasar spectra has been the only tracer of large-scale structures producing measurements of baryon acoustic oscillations (BAO) at redshifts above 2. Given the higher redshifts and the smaller scales probed, the clustering of the forest also yielded competitive constrains on the sum of the mass of the neutrino species, when combining it with measurements of the cosmic microwave background (CMB) anisotropies. Current and future spectroscopic surveys plan to observe denser samples of Lyα forests to improve our understanding of the $z > 2$ Universe.

In this chapter, I expose my contributions to the study of dark energy through Lyα forest observations. Section 3.1 introduce the main concepts used in this chapter. Section 3.2 focus on the BAO measurements from BOSS and eBOSS surveys for which I provided key contributions. My thesis[1] was dedicated to this topic. Section 3.3 and 3.4 present two projects carried out by my former PhD student Samantha Youles at the University of Portsmouth, UK, who graduated on the 18th of March 2022.

3.1 Forests as a tracer of the Universe's structures

The Lyα forest is the name for a series of absorption lines observed in quasar spectra caused by the presence of neutral hydrogen along the line of sight between us and the quasars. Figure **XX** shows an example of a optical quasar spectrum with its Lyα forest. These lines are seen bluewards of the Lyα emission peak of the quasar, which lies at the quasar rest-frame wavelength $\lambda_{\rm rest} = 1216$ Å. The absorption is not limited to the first transition; bluewards of the Lyβ peak ($\lambda_{\rm rest} = 1025$ Å) we also observe Lyβ absorption lines on top of the Lyα ones, and similarly for all Lyman series until the Lyman break at 912 Å.

The advatage of the forests is that it provides a tomographic view of the matter distribution along the line of sight of the quasar. This is because, as the light propagates outwards of the quasar, the Universe expands, causing the whole spectrum to be redshifted. When the redshifted spectrum hits a hydrogen atom, the light being absorbed at the Lyα transition in the *atom* rest-frame is no longer at the Lyα wavelength in the *quasar* rest-frame: it a bluer

[1] https://tel.archives-ouvertes.fr/tel-01389967

wavelength. If a given quasar sits at a redshift z_q and a given intervening atom sits at a redshift $z_a < z_q$, the Lyα photon being absorbed by the atom corresponds to a photon at $\lambda_{\rm rest} = 1216(1+z_a)/(1+z_q)$ Å in the quasar rest-frame. In our frame, the observed wavelength of the atom absorption, or equivalently of its Lyα line, is $\lambda_{\rm obs} = 1216(1+z_a)$ Å. Note the observed wavelength does not depend on the quasar redshift. We only need the quasar redshift to identify where the Lyα forest is in the observed spectrum, such that we can assign each observed wavelength to a quasar rest-frame wavelength. The result is that a single forest of lines maps the neutral hydrogen density accros a large range in redshifts. One single quasar spectrum can yield a map of the large-scale distribution of matter along its line of sight over up to several hundreds of megaparsecs (Mpc).

How much neutral hydrogen is needed to create a forest of Lyα absorption lines? Not a lot as it turns out. Given the high cross-section of the Lyα resonance, very low densities of neutral hydrogen are sufficient to create a line. At redshifts $2 < z < 4$ where Lyα forests are observed in the optical, typical densities found in the intergalactic medium (IGM), $n_{\rm HI} \sim 10^{XXX}$ cm^{-3}, are enough to absorb a significant fraction of the photons. Denser regions completely absorb the light and create saturated lines (zero flux). This is the case of the so-called *high-column density systems* (HCDs), which are often associated with galaxies or proto-galaxies. The extreme cases can be observed with high-resolution spectrocopy, where we can also observe a non-saturated *deuterium* absorption from which we derive constraints on big-bang nucleosynthesis (BBN, see section 1.5.3).

The Lyα forest, and therefore the amounts of neutral hydrogen in the IGM, is tighly connected with the process of reionisation of the Universe. As more stars and quasars form, more ultraviolet light is produced, progressively ionising the neutral hydrogen. On top of that, the Universe continuously expands, diluting it. Thus, the average absorption of forests decreases with time, or increases with redshift. At redshifts above 6, most of the light bluewards of the Lyα emission is absorbed, while at redshifts below 1, the Lyα absorption is minimal. Forests from $z_q > 6$ quasars are used to put constraints on reionisation (ref?).

The Lyα forest and its connection with the large-scale structures have been studied theoretically since works by James E. Gunn et al. 1965. Most of recent advances are thanks to numerical simulations. In order to simulate forests, a full hydrodynamic n-body simulations are required, including all the complex baryonic physics. **Add more refs.** On large scales, it has been shown that the forest can be considered as linear tracer of the underlying matter field McDonald, Miralda-Escudé, et al. 2000; McDonald 2003; McDonald, Seljak, Cen, et al. 2005. On smaller scales, the gas physics is more complex to model given the effects of pressure and thermal velocities. Feedback from supernovae explosions, AGN or star forming galaxies also play an important role to model the small-scale clustering (Chabanier et al. 2020). The small scales are interesting due to their potential to constrain neutrino masses for instance.

The first measurements of clustering using the Lyα forests were based solely on the two-point statistics along the same line of sight (Croft et al. 1999; McDonald, Seljak, Burles, et al. 2006). Given the good wavelength sampling of a forest, limited by the resolution of our spectrographs, the small scales are easily accessible in the radial/wavelength direction. This type of measurement is still performed today and allow us to obtain tight upper limits on the total mass of neutrino species (Nathalie Palanque-Delabrouille et al. 2020), when combined with measurements of the cosmic microwave background.

It is only with the Baryon Oscillation Spectroscopic Survey (BOSS) from SDSS-III that we could study the clustering of Lyα forests in three dimensions. Thanks to the density of quasars observed by BOSS, of about 15 deg^{-2}, it was possible for the first time to estimate correlations using absorption from neighboring lines of sight. Also thanks to the large area of sky covered by BOSS, the first measurement of baryon acoustic oscillations (BAO) using forests was achieved Busca et al. 2013; Slosar, Iršič, et al. 2013; Kirkby et al. 2013.

Quasars also trace the matter field. While their density is not homogenous enough across the sky to measure clustering using these quasars alone, they can be cross-correlated with the forests. The cross-correlation between quasars and Lyα forests is interesting because it is mostly independent of the Lyα forest auto-correlation. This is mainly because the quasar sample has a low density (shot-noise dominated). The first measurement of BAO in the quasar-forest cross-correlation was also possible with BOSS (Font-Ribera, Kirkby, et al. 2014). The BAO constraints from the auto and cross correlations could be combined assuming that these two are independent.

Since the first measurements of BAO using forests, the BOSS and eBOSS collaborations published BAO constraints with increasingly larger samples and improved analysis. They are associated with the official SDSS Data Releases (DR):

- DR9: First measurement of large-scale Lyα correlations without BAO (Slosar, Font-Ribera, et al. 2011);
- DR9: First detection of BAO in the Lyα auto-correlation (Busca et al. 2013; Slosar, Iršič, et al. 2013; Kirkby et al. 2013);
- DR11: First detection of BAO in the quasar- Lyα cross-correlation (Font-Ribera, Kirkby, et al. 2014), updated auto-correlation measurement (Delubac et al. 2015);
- DR12: Final BOSS auto-correlation (Julian E. Bautista et al. 2017) and cross-correlation measurements (du Mas des Bourboux, Le Goff, et al. 2017);
- DR14: Updated measurements with eBOSS data (de Sainte Agathe et al. 2019; Blomqvist et al. 2019);
- DR16: Final Lyα BAO measurements of SDSS (du Mas des Bourboux, Rich, et al. 2020).

3.2 Baryon acoustic oscillations in the forests

In this section I detail the methodology I used in my past work to measure BAO with a set of Lyα forests, highlighting my personal contributions. I consider the case of SDSS forests, which are observed in the optical domain with low-resolution spectroscopy. Forest have a rather low signal-to-noise ratio on average, so the methods are fit to this type of data. Similar methods are employed in the measurement of the line-of-sight (or one-dimensionnal) power-spectrum, but we focus on BAO here.

The main steps of the BAO analysis with Lyα forests are:

- estimate of the transmission field and their associated weights;
- estimate of the two-point correlation functions, including the cross-correlation with quasars;
- estimate of correction matrices due to distortions of continuum fitting and metals;
- fit of the BAO model over measured correlations.

3.2.1 Transmission field

As described in section 3.1, the amount of absorbed flux at a given wavelength (redshift) is related to the density of neutral hydrogen and therefore is a tracer of structures.

The main observable used to compute correlations is the so-called *transmission* F, defined as

$$F(\hat{n},\lambda) = f(\hat{n},\lambda)/C(\hat{n},\lambda) = \exp\{-\tau(\hat{n},\lambda)\} \tag{3.1}$$

where $f(\hat{n},\lambda)$ is the observed flux and $C(\hat{n},\lambda)$ is the unabsorbed/original flux level, for a quasar line-of-sight at angular position $\hat{n}$ and observer-frame wavelength λ, which can be linked to the absorber redshift $z = \lambda/\lambda_\alpha - 1$ if the absorption is due to Lyα. We can also express the transmission as a function of the optical depth τ as in the right-hand side of Eq. 3.1.

The challenge is to estimate transmissions from the observed fluxes of a set of quasar spectra, particularly given that our data is low-resolution and relatively noisy. This makes it hard to "see" the unabsorbed flux level C, also known as the *continuum* level, requiring automated methods. Several past attemps to achive this used either principal-component analysis techniques (Lee et al. 2012) where the templates were built from high-resolution and high signal-to-noise data; or maximum likelihood methods accounting for the non-Gaussian nature of the probability density function of F (Busca et al. 2013). During my PhD, I particularly tried to merge these last two methods into a single one, without success. Those methods, while more sophisticated and flexible in their modelling of C, they suffer from the additional noise added to the estimated transmission due to noisier estimates of C. The simplest method will prevail in the latest analyses, which consists in averaging forests in their rest-frame to obtain a single average shape for C, or *mean continuum* $\bar{C}$. This shape is then fitted to each individual forest with a linear tilt in $\log\lambda$, i.e., $C(\hat{n},\lambda) \equiv \bar{C}(\lambda)[a_0(\hat{n}) + a_1(\hat{n})\log\lambda]$, where a_0 and a_1 are fitted coefficients per quasar.

Once the continnum level C is estimated for each forest, one can compute the transmission F and their *fluctuations* δ_F around the mean, defined as

$$\delta_F(\hat{n},\lambda) = \frac{F(\hat{n},\lambda)}{\langle F\rangle} - 1 \tag{3.2}$$

where $\langle F\rangle$ is the ensemble-averaged transmission of the Universe.

The $\langle F\rangle$ is actually an evolving function of time (or redshift or observed-frame wavelength) and it is important to take this evolution into account when computing δ_F. Several measurements of this quantity exist (Faucher-Giguère et al. 2008; Pâris et al. 2011; Becker et al. 2013; Kamble et al. 2020), thought the latest BAO measurements do not use them directly to compute δ_F. One could in principle use the forests themselves to estimate $\langle F\rangle$, by stacking forests in their observer-frame (by contrast with the mean continuum that is a stack in the quasar rest-frame), though this requires a good estimate of C. If one express δ_F as a function of the observed flux f, the continuum C and the average transmission $\langle F\rangle$, one sees that there are degeneracies. The latest BAO analyses therefore fits a linear function that models the product $C\langle F\rangle$ simultaneously.

All methods to estimate the transmission fluctuations also suffer from the fact that they use information the forests themselves to estimate C or $C\langle F\rangle$. This creates spurious correlations between a given pixel in a given forest and a neighboring pixel in the same forest. As I will discuss in section 3.2.3, spurious correlations are also introduced between pixels in different lines-of-sight, distorting the correlation function. We name this effect the *distortion by continuum fitting*; it needs to be correctly modelled when fitting the correlation function.

Typical ranges chosen to define the Lyα forest and extract the transmission field are between 1040 and 1200 Å in the quasar rest-frame. Recent analyses also consider the Lyβ forest region, between 920 and 1020 Å, where both Lyα and Lyβ absorption are present. The absorption in this region can be assigned a redshift that depends on the choice of λ_{rest}, that can be either Lyα = 1216 Å or Lyβ = 1025 Å. These rest-frame wavelengths are separated enough such that both can be used in clustering measurements without much contamination at separations below $200h^{-1}$Mpc.

Uncertainties of the transmission fluctuations are also estimated from the data themselves. Typically two major components are taken into account when defining uncertainties: instrumental noise and the instrinsic variance of absorbers. The former is essentially the output of the data reduction pipeline, described in Chapter 2, corrected with some normalisation factor. The latter is estimated from the variance of δ_F observed in the data. The intrinsic variance of δ_F is an increasing function of redshift, while the instrumental noise is typically decreasing with observer-frame wavelength, since forest mostly lie at the blue end of the spectrographs. The inverse of the final pixel uncertainty squared is used as a weight in the estimates of the correlation function.

Word on DLAs ?

3.2.2 Two-point correlation functions

Once the transmission fluctuations δ_F and their weights w are estimated for all pixels of all forests, we compute their auto-correlation function and their cross-correlation with quasars (or any other point tracer) in three dimensions, as a function of comoving radial and transverse separations.

The first step is to convert redshifts to comoving distances using a fiducial cosmology. With angular positions and distances, we can obtain the separation $\vec{r} = (r_\perp, r_\parallel)$ between two tracers, where $r_\perp$ is the component orthogonal to the line-of-sight and $r_\parallel$ is the component along the line-of-sight.

The correlations are estimated in bins of separation. We consider usually bins of $4h^{-1}$Mpc from 0 to $200h^{-1}$Mpcin both radial and transverse directions. For the cross-correlation with quasars, the radial separation can be negative, meaning that the absorber is closer than the quasar from us. Let A be the index of a separation bin, the auto-correlation is defined as

$$\xi_A^{\text{auto}} = \frac{\sum_{i,j \text{ if } \vec{r}_{ij} \in A} w_i w_j \delta_{F,i} \delta_{F,j}}{\sum_{i,j \text{ if } \vec{r}_{ij} \in A} w_i w_j} \tag{3.3}$$

where the indexes i, j denote a given pixel in the forest. The sum is over all pairs of absorbers for which the separation $\vec{r}_{ij} = \vec{r}_i - \vec{r}_j$ falls inside bin A.

The cross-correlation of absorbers with quasars is estimated with the following estimator:

$$\xi_A^{\text{cross}} = \frac{\sum_{i,j \text{ if } \vec{r}_{ij} \in A} w_i w_j \delta_{F,i}}{\sum_{i,j \text{ if } \vec{r}_{ij} \in A} w_i w_j}, \tag{3.4}$$

which is very similar to the auto-correlation one in Eq. 3.3. The index i runs over absorbers while j runs over quasars, but there is no $\delta_{F,j}$ term. This estimator is valid under a few assumptions: sparcity of quasars, weak cross-correlation and weak auto-correlation. These assumptions are discussed in detail in the appendix B of Font-Ribera, Miralda-Escudé, et al. 2012.

The covariance matrix is estimated using sub-samples of the full survey. Under the assumption that each sub-sample s is independent, the estimator of the covariance between ξ_A and ξ_B is

$$C_{AB} = \frac{1}{W_A W_B} \sum_s W_A^s W_B^s [\xi_A^s \xi_B^s - \xi_A \xi_B], \tag{3.5}$$

where W_A^s is the total weight in bin A of sub-sample s and $W_A \equiv \sum_s W_A^s$. This estimator has been tested with 100 realisations of synthetic datasets (mocks) and it shows to be robust at the current precision level.

The data vector contains around 50x50 bins, making the covariance too large (2500x2500) for the usual number of available sub-samples (~ 1000). To avoid the matrix to be singular, we apply a smoothing to it. The smoothing procedure considers that the correlation coefficients, defined as $\rho_{AB} = C_{AB}/\sqrt{C_{AA}C_{BB}}$, are only a function of $\Delta r_\perp \equiv r_{\perp B} - r_{\perp A}$ and $\Delta r_\parallel \equiv r_{\parallel B} - r_{\parallel A}$. By averaging all correlation coefficients with the same $(\Delta r_\perp, \Delta r_\parallel)$, we obtain a 50x50 matrix which is now positive definite. The new covariance matrix is constructed by taking these averaged coefficients and multiplying them by the variances. This method is used to estimate covariance matrices for both auto and cross correlation functions, but also for the cross-covariance between $\xi_A^{\rm auto}$ and $\xi_B^{\rm cross}$, used in joint fits (see section 3.2.4).

3.2.3 Correction matrices

There are two important effects to be taken into account when modelling the Lyα correlation functions: the distortion by the continuum fitting, discussed in section 3.2.1, and the contamination by metal absorption. The most recent analyses use matrices to convolve a binned cosmological model and obtain the final template to be compared to the measured binned correlations.

3.2.4 BAO model

3.3 Impact of redshift errors

3.4 Weak-lensing of forests

4 The mid-redshift Universe and its galaxies

Contents

4.1 Galaxies as a tracer of the matter field 35
4.2 Baryon acoustic oscillations with galaxies 35
4.3 Redshift-space distortions 35
4.4 Cross-correlation with radio surveys 35

At redshifts between 0 and 2, galaxies can be used as tracers of the matter distribution.

4.1 Galaxies as a tracer of the matter field

4.2 Baryon acoustic oscillations with galaxies

4.3 Redshift-space distortions

4.4 Cross-correlation with radio surveys

5 The low-redshift Universe and its velocities

Contents

5.1 Measuring peculiar velocities 36
5.2 Combining velocities with densities 36
5.3 Testing general relativity with velocities 36

At low redshifts, below 0.1, peculiar velocities can be directly measured and their statistical properties can provide more information about a gravity on large scales.

5.1 Measuring peculiar velocities

5.2 Combining velocities with densities

5.3 Testing general relativity with velocities

Conclusion

Lorem ipsum dolor sit amet, consectetuer adipiscing elit. Ut purus elit, vestibulum ut, placerat ac, adipiscing vitae, felis. Curabitur dictum gravida mauris. Nam arcu libero, nonummy eget, consectetuer id, vulputate a, magna. Donec vehicula augue eu neque. Pellentesque habitant morbi tristique senectus et netus et malesuada fames ac turpis egestas. Mauris ut leo. Cras viverra metus rhoncus sem. Nulla et lectus vestibulum urna fringilla ultrices. Phasellus eu tellus sit amet tortor gravida placerat. Integer sapien est, iaculis in, pretium quis, viverra ac, nunc. Praesent eget sem vel leo ultrices bibendum. Aenean faucibus. Morbi dolor nulla, malesuada eu, pulvinar at, mollis ac, nulla. Curabitur auctor semper nulla. Donec varius orci eget risus. Duis nibh mi, congue eu, accumsan eleifend, sagittis quis, diam. Duis eget orci sit amet orci dignissim rutrum.

Nam dui ligula, fringilla a, euismod sodales, sollicitudin vel, wisi. Morbi auctor lorem non justo. Nam lacus libero, pretium at, lobortis vitae, ultricies et, tellus. Donec aliquet, tortor sed accumsan bibendum, erat ligula aliquet magna, vitae ornare odio metus a mi. Morbi ac orci et nisl hendrerit mollis. Suspendisse ut massa. Cras nec ante. Pellentesque a nulla. Cum sociis natoque penatibus et magnis dis parturient montes, nascetur ridiculus mus. Aliquam tincidunt urna. Nulla ullamcorper vestibulum turpis. Pellentesque cursus luctus mauris.

Bibliography

[Abb+17] B. P. Abbott et al. “A Gravitational-Wave Standard Siren Measurement of the Hubble Constant”. In: *Nature* 551.7678 (7678 2017), pp. 85–88. DOI: 10.1038/nature24471 (cit. on p. 17).

[Ahu+20] Romina Ahumada et al. “The 16th Data Release of the Sloan Digital Sky Surveys: First Release from the APOGEE-2 Southern Survey and Full Release of eBOSS Spectra”. In: *The Astrophysical Journal Supplement Series* 249 (1, 2020), p. 3. DOI: 10.3847/1538-4365/ab929e (cit. on p. 26).

[Aio+20] Simone Aiola et al. “The Atacama Cosmology Telescope: DR4 Maps and Cosmological Parameters”. In: *Journal of Cosmology and Astroparticle Physics* 2020.12 (30, 2020), pp. 047–047. DOI: 10.1088/1475-7516/2020/12/047 (cit. on p. 21).

[Ala+17] Shadab Alam, Metin Ata, Stephen Bailey, Florian Beutler, Dmitry Bizyaev, Jonathan A. Blazek, Adam S. Bolton, Joel R. Brownstein, Angela Burden, Chia-Hsun Chuang, Johan Comparat, Antonio J. Cuesta, Kyle S. Dawson, Daniel J. Eisenstein, Stephanie Escoffier, Héctor Gil-Marín, Jan Niklas Grieb, Nick Hand, Shirley Ho, Karen Kinemuchi, David Kirkby, Francisco Kitaura, Elena Malanushenko, Viktor Malanushenko, Claudia Maraston, Cameron K. McBride, Robert C. Nichol, Matthew D. Olmstead, Daniel Oravetz, Nikhil Padmanabhan, Nathalie Palanque-Delabrouille, Kaike Pan, Marcos Pellejero-Ibanez, Will J. Percival, Patrick Petitjean, Francisco Prada, Adrian M. Price-Whelan, Beth A. Reid, Sergio A. Rodríguez-Torres, Natalie A. Roe, Ashley J. Ross, Nicholas P. Ross, Graziano Rossi, Jose Alberto Rubiño-Martín, Shun Saito, Salvador Salazar-Albornoz, Lado Samushia, Ariel G. Sánchez, Siddharth Satpathy, David J. Schlegel, Donald P. Schneider, Claudia G. Scóccola, Hee-Jong Seo, Erin S. Sheldon, Audrey Simmons, Anže Slosar, Michael A. Strauss, Molly E. C. Swanson, Daniel Thomas, Jeremy L. Tinker, Rita Tojeiro, Mariana Vargas Magaña, Jose Alberto Vazquez, Licia Verde, David A. Wake, Yuting Wang, David H. Weinberg, Martin White, W. Michael Wood-Vasey, Christophe Yèche, Idit Zehavi, Zhongxu Zhai, and Gong-Bo Zhao. “The Clustering of Galaxies in the Completed SDSS-III Baryon Oscillation Spectroscopic Survey: Cosmological Analysis of the DR12 Galaxy Sample”. In: *Monthly Notices of the Royal Astronomical Society* 470 (1, 2017), pp. 2617–2652. DOI: 10.1093/mnras/stx721 (cit. on p. 22).

[Ala+21] Shadab Alam, Marie Aubert, Santiago Avila, Christophe Balland, Julian E. Bautista, Matthew A. Bershady, Dmitry Bizyaev, Michael R. Blanton, Adam S. Bolton, Jo Bovy, Jonathan Brinkmann, Joel R. Brownstein, Etienne Burtin, Solène Chabanier, Michael J. Chapman, Peter Doohyun Choi, Chia-Hsun Chuang, Johan Comparat, Marie-Claude Cousinou, Andrei Cuceu, Kyle S. Dawson, Sylvain de la Torre, Arnaud de Mattia, Victoria de Sainte Agathe, Hélion du Mas des Bourboux, Stephanie Escoffier, Thomas Etourneau, James Farr, Andreu Font-Ribera, Peter M. Frinchaboy, Sebastien Fromenteau, Héctor Gil-Marín, Jean-Marc Le Goff, Alma X. Gonzalez-Morales, Violeta Gonzalez-Perez, Kathleen Grabowski, Julien Guy, Adam J. Hawken, Jiamin Hou, Hui Kong, James Parker, Mark Klaene, Jean-Paul Kneib, Sicheng Lin, Daniel Long, Brad W. Lyke, Axel de la Macorra, Paul Martini, Karen Masters, Faizan G. Mohammad, Jeongin Moon, Eva-Maria Mueller, Andrea Muñoz-Gutiérrez, Adam D. Myers, Seshadri Nadathur, Richard Neveux, Jeffrey A. Newman, Pasquier Noterdaeme, Audrey Oravetz, Daniel Oravetz, Nathalie Palanque-Delabrouille, Kaike Pan, Romain Paviot, Will J. Percival, Ignasi Pérez-Ràfols, Patrick Petitjean, Matthew M. Pieri, Abhishek Prakash, Anand Raichoor, Corentin Ravoux, Mehdi Rezaie, James Rich, Ashley J. Ross, Graziano Rossi, Rossana Ruggeri, Vanina Ruhlmann-Kleider, Ariel G. Sánchez, F. Javier Sánchez, José R. Sánchez-Gallego, Conor Sayres, Donald P. Schneider, Hee-Jong Seo, Arman Shafieloo, Anže Slosar, Alex Smith, Julianna Stermer, Amelie Tamone, Jeremy L. Tinker, Rita Tojeiro, Mariana Vargas-Magaña, Andrei Variu, Yuting Wang, Benjamin A. Weaver, Anne-Marie Weijmans, Christophe Yèche, Pauline Zarrouk, Cheng Zhao, Gong-Bo Zhao, and Zheng Zheng. "Completed SDSS-IV Extended Baryon Oscillation Spectroscopic Survey: Cosmological Implications from Two Decades of Spectroscopic Surveys at the Apache Point Observatory". In: *Physical Review D* 103.8 (28, 2021), p. 083533. DOI: `10.1103/PhysRevD.103.083533` (cit. on pp. 20, 22).

[Ave+21] Erik Aver, Danielle A. Berg, Keith A. Olive, Richard W. Pogge, John J. Salzer, and Evan D. Skillman. "Improving Helium Abundance Determinations with Leo P as a Case Study". In: *Journal of Cosmology and Astroparticle Physics* 2021.03 (1, 2021), p. 027. DOI: `10.1088/1475-7516/2021/03/027` (cit. on p. 19).

[Ayl+17] K. Aylor, Z. Hou, L. Knox, K. T. Story, B. A. Benson, L. E. Bleem, J. E. Carlstrom, C. L. Chang, H.-M. Cho, R. Chown, T. M. Crawford, A. T. Crites, T. de Haan, M. A. Dobbs, W. B. Everett, E. M. George, N. W. Halverson, N. L. Harrington, G. P. Holder, W. L. Holzapfel, J. D. Hrubes, R. Keisler, A. T. Lee, E. M. Leitch, D. Luong-Van, D. P. Marrone, J. J. McMahon, S. S. Meyer, M. Millea, L. M. Mocanu, J. J. Mohr, T. Natoli, Y. Omori, S. Padin, C. Pryke, C. L. Reichardt, J. E. Ruhl, J. T. Sayre, K. K. Scaffer, E. Shirokoff, Z. Staniszewski, A. A. Stark, K. Vanderlinde, J. D. Vieira, and R. Williamson. "A Comparison of Cosmological Parameters Determined from CMB Temperature Power Spectra from the South Pole Telescope and the Planck Satellite". In: *The Astrophysical Journal* 850.1 (21, 2017), p. 101. DOI: `10.3847/1538-4357/aa947b` (cit. on p. 21).

[Bal+00] A. Balbi, P. Ade, J. Bock, J. Borrill, A. Boscaleri, P. De Bernardis, P. G. Ferreira, S. Hanany, V. Hristov, A. H. Jaffe, A. T. Lee, S. Oh, E. Pascale, B. Rabii, P. L. Richards, G. F. Smoot, R. Stompor, C. D. Winant, and J. H. P. Wu. "Constraints on Cosmological Parameters from MAXIMA-1". In: *The Astrophysical Journal* 545 (1, 2000), pp. L1–L4. DOI: `10.1086/317323` (cit. on p. 9).

[Bal+21] L. Balkenhol et al. "Constraints on ΛCDM Extensions from the SPT-3G 2018 EE and TE Power Spectra". In: *Physical Review D* 104.8 (4, 2021), p. 083509. DOI: `10.1103/PhysRevD.104.083509` (cit. on p. 21).

[Bau+20] Julian E Bautista, Romain Paviot, Mariana Vargas Magaña, Sylvain de la Torre, Sebastien Fromenteau, Hector Gil-Marín, Ashley J Ross, Etienne Burtin, Kyle S Dawson, Jiamin Hou, Jean-Paul Kneib, Arnaud de Mattia, Will J Percival, Graziano Rossi, Rita Tojeiro, Cheng Zhao, Gong-Bo Zhao, Shadab Alam, Joel Brownstein, Michael J Chapman, Peter D Choi, Chia-Hsun Chuang, Stéphanie Escoffier, Axel de la Macorra, Hélion du Mas des Bourboux, Faizan G Mohammad, Jeongin Moon, Eva-Maria Müller, Seshadri Nadathur, Jeffrey A Newman, Donald Schneider, Hee-Jong Seo, and Yuting Wang. "The Completed SDSS-IV Extended Baryon Oscillation Spectroscopic Survey: Measurement of the BAO and Growth Rate of Structure of the Luminous Red Galaxy Sample from the Anisotropic Correlation Function between Redshifts 0.6 and 1". In: *Monthly Notices of the Royal Astronomical Society* 500.1 (3, 2020), pp. 736–762. DOI: 10.1093/mnras/staa2800 (cit. on p. 22).

[Bau+17] Julian E. Bautista, Nicolás G. Busca, Julien Guy, James Rich, Michael Blomqvist, Hélion du Mas des Bourboux, Matthew M. Pieri, Andreu Font-Ribera, Stephen Bailey, Timothée Delubac, David Kirkby, Jean-Marc Le Goff, Daniel Margala, Anže Slosar, Jose Alberto Vazquez, Joel R. Brownstein, Kyle S. Dawson, Daniel J. Eisenstein, Jordi Miralda-Escudé, Pasquier Noterdaeme, Nathalie Palanque-Delabrouille, Isabelle Pâris, Patrick Petitjean, Nicholas P. Ross, Donald P. Schneider, David H. Weinberg, and Christophe Yèche. "Measurement of Baryon Acoustic Oscillation Correlations at z = 2.3 with SDSS DR12 Lyα-Forests". In: *Astronomy and Astrophysics* 603 (1, 2017), A12. DOI: 10.1051/0004-6361/201730533 (cit. on pp. 27, 31).

[Bec+13] George D. Becker, Paul C. Hewett, Gábor Worseck, and J. Xavier Prochaska. "A Refined Measurement of the Mean Transmitted Flux in the Lyα Forest over $2 < z < 5$ Using Composite Quasar Spectra". In: *Monthly Notices of the Royal Astronomical Society* 430 (1, 2013), pp. 2067–2081. DOI: 10.1093/mnras/stt031 (cit. on p. 32).

[Beu+12] Florian Beutler, Chris Blake, Matthew Colless, D. Heath Jones, Lister Staveley-Smith, Gregory B. Poole, Lachlan Campbell, Quentin Parker, Will Saunders, and Fred Watson. "The 6dF Galaxy Survey: z \approx 0 Measurement of the Growth Rate and Sigma_8". In: *Monthly Notices of the Royal Astronomical Society* 423.4 (11, 2012), pp. 3430–3444. DOI: 10.1111/j.1365-2966.2012.21136.x (cit. on p. 20).

[BIC+21] BICEP/Keck et al. "A Demonstration of Improved Constraints on Primordial Gravitational Waves with Delensing". In: *Physical Review D* 103.2 (26, 2021), p. 022004. DOI: 10.1103/PhysRevD.103.022004 (cit. on p. 21).

[Bir+20] S. Birrer, A. J. Shajib, A. Galan, M. Millon, T. Treu, A. Agnello, M. Auger, G. C.-F. Chen, L. Christensen, T. Collett, F. Courbin, C. D. Fassnacht, L. V. E. Koopmans, P. J. Marshall, J.-W. Park, C. E. Rusu, D. Sluse, C. Spiniello, S. H. Suyu, S. Wagner-Carena, K. C. Wong, M. Barnabè, A. S. Bolton, O. Czoske, X. Ding, J. A. Frieman, and L. Van de Vyvere. "TDCOSMO - IV. Hierarchical Time-Delay Cosmography – Joint Inference of the Hubble Constant and Galaxy Density Profiles". In: *Astronomy & Astrophysics* 643 (1, 2020), A165. DOI: 10.1051/0004-6361/202038861 (cit. on p. 17).

[Bla+17] Michael R. Blanton, Matthew A. Bershady, et al. "Sloan Digital Sky Survey IV: Mapping the Milky Way, Nearby Galaxies, and the Distant Universe". In: *The Astronomical Journal* 154.1 (2017), p. 28. DOI: 10.3847/1538-3881/aa7567 (cit. on p. 20).

[Bla+03] Michael R. Blanton, Huan Lin, Robert H. Lupton, F. Miller Maley, Neal Young, Idit Zehavi, and Jon Loveday. "An Efficient Targeting Strategy for Multiobject Spectrograph Surveys: The Sloan Digital Sky Survey "Tiling" Algorithm". In: *The Astronomical Journal* 125 (1, 2003), pp. 2276–2286. DOI: 10.1086/344761 (cit. on p. 26).

[Blo+19] Michael Blomqvist, Hélion du Mas des Bourboux, Nicolás G. Busca, Victoria de Sainte Agathe, James Rich, Christophe Balland, Julian E. Bautista, Kyle Dawson, Andreu Font-Ribera, Julien Guy, Jean-Marc Le Goff, Nathalie Palanque-Delabrouille, Will J. Percival, Ignasi Pérez-Ràfols, Matthew M. Pieri, Donald P. Schneider, Anže Slosar, and Christophe Yèche. "Baryon Acoustic Oscillations from the Cross-Correlation of Lyα Absorption and Quasars in eBOSS DR14". In: *Astronomy and Astrophysics* 629 (2019), A86. DOI: 10.1051/0004-6361/201935641 (cit. on p. 31).

[Bro+19a] D. Brout, M. Sako, D. Scolnic, R. Kessler, C. B. D'Andrea, T. M. Davis, S. R. Hinton, A. G. Kim, J. Lasker, E. Macaulay, A. Möller, R. C. Nichol, M. Smith, M. Sullivan, R. C. Wolf, S. Allam, B. A. Bassett, P. Brown, F. J. Castander, M. Childress, R. J. Foley, L. Galbany, K. Herner, E. Kasai, M. March, E. Morganson, P. Nugent, Y.-C. Pan, R. C. Thomas, B. E. Tucker, W. Wester, T. M. C. Abbott, J. Annis, S. Avila, E. Bertin, D. Brooks, D. L. Burke, A. Carnero Rosell, M. Carrasco Kind, J. Carretero, M. Crocce, C. E. Cunha, L. N. da Costa, C. Davis, J. De Vicente, S. Desai, H. T. Diehl, P. Doel, T. F. Eifler, B. Flaugher, P. Fosalba, J. Frieman, J. García-Bellido, E. Gaztanaga, D. W. Gerdes, D. A. Goldstein, D. Gruen, R. A. Gruendl, J. Gschwend, G. Gutierrez, W. G. Hartley, D. L. Hollowood, K. Honscheid, D. J. James, K. Kuehn, N. Kuropatkin, O. Lahav, T. S. Li, M. Lima, J. L. Marshall, P. Martini, R. Miquel, B. Nord, A. A. Plazas, A. Roodman, E. S. Rykoff, E. Sanchez, V. Scarpine, R. Schindler, M. Schubnell, S. Serrano, I. Sevilla-Noarbe, M. Soares-Santos, F. Sobreira, E. Suchyta, M. E. C. Swanson, G. Tarle, D. Thomas, D. L. Tucker, A. R. Walker, B. Yanny, Y. Zhang, and DES COLLABORATION. "First Cosmology Results Using Type Ia Supernovae from the Dark Energy Survey: Photometric Pipeline and Light-curve Data Release". In: *The Astrophysical Journal* 874 (1, 2019), p. 106. DOI: 10.3847/1538-4357/ab06c1 (cit. on p. 18).

[Bro+19b] D. Brout, D. Scolnic, et al. "First Cosmology Results Using SNe Ia from the Dark Energy Survey: Analysis, Systematic Uncertainties, and Validation". In: *The Astrophysical Journal* 874.2 (2019), p. 150. DOI: 10.3847/1538-4357/ab08a0 (cit. on p. 18).

[Bus+13] N. G. Busca, T. Delubac, J. Rich, S. Bailey, A. Font-Ribera, D. Kirkby, J.-M. Le Goff, M. M. Pieri, A. Slosar, É. Aubourg, J. E. Bautista, D. Bizyaev, M. Blomqvist, A. S. Bolton, J. Bovy, H. Brewington, A. Borde, J. Brinkmann, B. Carithers, R. A. C. Croft, K. S. Dawson, G. Ebelke, D. J. Eisenstein, J.-C. Hamilton, S. Ho, D. W. Hogg, K. Honscheid, K.-G. Lee, B. Lundgren, E. Malanushenko, V. Malanushenko, D. Margala, C. Maraston, K. Mehta, J. Miralda-Escudé, A. D. Myers, R. C. Nichol, P. Noterdaeme, M. D. Olmstead, D. Oravetz, N. Palanque-Delabrouille, K. Pan, I. Pâris, W. J. Percival, P. Petitjean, N. A. Roe, E. Rollinde, N. P. Ross, G. Rossi, D. J. Schlegel, D. P. Schneider, A. Shelden, E. S. Sheldon, A. Simmons, S. Snedden, J. L. Tinker, M. Viel, B. A. Weaver, D. H. Weinberg, M. White, C. Yèche, and D. G. York. "Baryon Acoustic Oscillations in the Lyα Forest of BOSS Quasars".

In: *Astronomy and Astrophysics* 552 (1, 2013), A96. DOI: 10.1051/0004-6361/201220724 (cit. on pp. 31, 32).

[Cha+20] Solène Chabanier, Frédéric Bournaud, Yohan Dubois, Nathalie Palanque-Delabrouille, Christophe Yèche, Eric Armengaud, Sébastien Peirani, and Ricarda Beckmann. "The Impact of AGN Feedback on the 1D Power Spectra from the Ly α Forest Using the Horizon-AGN Suite of Simulations". In: *Monthly Notices of the Royal Astronomical Society* 495 (1, 2020), pp. 1825–1840. DOI: 10.1093/mnras/staa1242 (cit. on p. 30).

[Cha98] B. Chaboyer. "The Age of the Universe." In: *Physics Reports* 307 (1, 1998), pp. 23–30. DOI: 10.1016/S0370-1573(98)00054-4 (cit. on p. 10).

[CP01] Michel Chevallier and David Polarski. "Accelerating Universes with Scaling Dark Matter". In: *International Journal of Modern Physics D* 10 (1, 2001), pp. 213–223. DOI: 10.1142/S0218271801000822 (cit. on p. 12).

[Col+05] Shaun Cole, Will J. Percival, John A. Peacock, Peder Norberg, Carlton M. Baugh, Carlos S. Frenk, Ivan Baldry, Joss Bland-Hawthorn, Terry Bridges, Russell Cannon, Matthew Colless, Chris Collins, Warrick Couch, Nicholas J. G. Cross, Gavin Dalton, Vincent R. Eke, Roberto De Propris, Simon P. Driver, George Efstathiou, Richard S. Ellis, Karl Glazebrook, Carole Jackson, Adrian Jenkins, Ofer Lahav, Ian Lewis, Stuart Lumsden, Steve Maddox, Darren Madgwick, Bruce A. Peterson, Will Sutherland, and Keith Taylor. "The 2dF Galaxy Redshift Survey: Power-Spectrum Analysis of the Final Data Set and Cosmological Implications". In: *Monthly Notices of the Royal Astronomical Society* 362 (1, 2005), pp. 505–534. DOI: 10.1111/j.1365-2966.2005.09318.x (cit. on p. 10).

[Col+21] DES Collaboration et al. "Dark Energy Survey Year 3 Results: Cosmological Constraints from Galaxy Clustering and Weak Lensing". 27, 2021 (cit. on p. 23).

[CC17] The LIGO Scientific Collaboration and The Virgo Collaboration. "GW170817: Observation of Gravitational Waves from a Binary Neutron Star Inspiral". In: *Physical Review Letters* 119.16 (16, 2017), p. 161101. DOI: 10.1103/PhysRevLett.119.161101 (cit. on p. 17).

[CtV16] The LIGO Scientific Collaboration and the Virgo Collaboration. "Observation of Gravitational Waves from a Binary Black Hole Merger". In: *Physical Review Letters* 116.6 (11, 2016), p. 061102. DOI: 10.1103/PhysRevLett.116.061102 (cit. on p. 17).

[Cro+99] Rupert A. C. Croft, David H. Weinberg, Max Pettini, Lars Hernquist, and Neal Katz. "The Power Spectrum of Mass Fluctuations Measured from the LYalpha Forest at Redshift Z=2.5". In: *The Astrophysical Journal* 520 (1, 1999), pp. 1–23. DOI: 10.1086/307438; (cit. on p. 30).

[dBer+00] P. de Bernardis, P. A. R. Ade, J. J. Bock, J. R. Bond, J. Borrill, A. Boscaleri, K. Coble, B. P. Crill, G. De Gasperis, P. C. Farese, P. G. Ferreira, K. Ganga, M. Giacometti, E. Hivon, V. V. Hristov, A. Iacoangeli, A. H. Jaffe, A. E. Lange, L. Martinis, S. Masi, P. V. Mason, P. D. Mauskopf, A. Melchiorri, L. Miglio, T. Montroy, C. B. Netterfield, E. Pascale, F. Piacentini, D. Pogosyan, S. Prunet, S. Rao, G. Romeo, J. E. Ruhl, F. Scaramuzzi, D. Sforna, and N. Vittorio. "A Flat Universe from High-Resolution Maps of the Cosmic Microwave Background Radiation". In: *Nature* 404 (1, 2000), pp. 955–959. DOI: 10.1038/35010035 (cit. on p. 9).

[Del+15] Timothée Delubac, Julian E. Bautista, Nicolás G. Busca, James Rich, David Kirkby, Stephen Bailey, Andreu Font-Ribera, Anže Slosar, Khee-Gan Lee, Matthew M. Pieri, Jean-Christophe Hamilton, Éric Aubourg, Michael Blomqvist, Jo Bovy, Jon Brinkmann, William Carithers, Kyle S. Dawson, Daniel J. Eisenstein, Satya Gontcho A. Gontcho, Jean-Paul Kneib, Jean-Marc Le Goff, Daniel Margala, Jordi Miralda-Escudé, Adam D. Myers, Robert C. Nichol, Pasquier Noterdaeme, Ross O'Connell, Matthew D. Olmstead, Nathalie Palanque-Delabrouille, Isabelle Pâris, Patrick Petitjean, Nicholas P. Ross, Graziano Rossi, David J. Schlegel, Donald P. Schneider, David H. Weinberg, Christophe Yèche, and Donald G. York. "Baryon Acoustic Oscillations in the Lyα Forest of BOSS DR11 Quasars". In: *Astronomy and Astrophysics* 574 (1, 2015), A59. DOI: 10.1051/0004-6361/201423969 (cit. on p. 31).

[dMat+21] Arnaud de Mattia, Vanina Ruhlmann-Kleider, Anand Raichoor, Ashley J. Ross, Amélie Tamone, Cheng Zhao, Shadab Alam, Santiago Avila, Etienne Burtin, Julian Bautista, Florian Beutler, Jonathan Brinkmann, Joel R. Brownstein, Michael J. Chapman, Chia-Hsun Chuang, Johan Comparat, Hélion du Mas des Bourboux, Kyle S. Dawson, Axel de la Macorra, Héctor Gil-Marín, Violeta Gonzalez-Perez, Claudio Gorgoni, Jiamin Hou, Hui Kong, Sicheng Lin, Seshadri Nadathur, Jeffrey A. Newman, Eva-Maria Mueller, Will J. Percival, Mehdi Rezaie, Graziano Rossi, Donald P. Schneider, Prabhakar Tiwari, M. Vivek, Yuting Wang, and Gong-Bo Zhao. "The Completed SDSS-IV Extended Baryon Oscillation Spectroscopic Survey: Measurement of the BAO and Growth Rate of Structure of the Emission Line Galaxy Sample from the Anisotropic Power Spectrum between Redshift 0.6 and 1.1". In: *Monthly Notices of the Royal Astronomical Society* 501 (1, 2021), pp. 5616–5645. DOI: 10.1093/mnras/staa3891 (cit. on p. 22).

[dSai+19] Victoria de Sainte Agathe, Christophe Balland, Hélion du Mas des Bourboux, Nicolás G. Busca, Michael Blomqvist, Julien Guy, James Rich, Andreu Font-Ribera, Matthew M. Pieri, Julian E. Bautista, Kyle Dawson, Jean-Marc Le Goff, Axel de la Macorra, Nathalie Palanque-Delabrouille, Will J. Percival, Ignasi Pérez-Ràfols, Donald P. Schneider, Anže Slosar, and Christophe Yèche. "Baryon Acoustic Oscillations at z = 2.34 from the Correlations of Lyα Absorption in eBOSS DR14". In: *Astronomy and Astrophysics* 629 (2019), A85. DOI: 10.1051/0004-6361/201935638 (cit. on p. 31).

[DS20] Scott Dodelson and Fabian Schmidt. *Modern Cosmology - 2nd Edition*. 2nd ed. Elsevier, 18, 2020 (cit. on p. 21).

[Doi+10] Mamoru Doi, Masayuki Tanaka, Masataka Fukugita, James E. Gunn, Naoki Yasuda, Željko Ivezić, Jon Brinkmann, Ernst de Haars, S. J. Kleinman, Jurek Krzesinski, and R. French Leger. "Photometric Response Functions of the Sloan Digital Sky Survey Imager". In: *The Astronomical Journal* 139 (1, 2010), pp. 1628–1648. DOI: 10.1088/0004-6256/139/4/1628 (cit. on p. 24).

[dMas+20] Hélion du Mas des Bourboux Helion, James Rich, Andreu Font-Ribera, Victoria de Sainte Agathe, James Farr, Thomas Etourneau, Jean-Marc Le Goff, Andrei Cuceu, Christophe Balland, Julian E. Bautista, Michael Blomqvist, Jonathan Brinkmann, Joel R. Brownstein, Solène Chabanier, Edmond Chaussidon, Kyle Dawson, Alma X. González-Morales, Julien Guy, Brad W. Lyke, Axel de la Macorra, Eva-Maria Mueller, Adam D. Myers, Christian Nitschelm, Andrea Muñoz Gutiérrez, Nathalie

Palanque-Delabrouille, James Parker, Will J. Percival, Ignasi Pérez-Ràfols, Patrick Petitjean, Matthew M. Pieri, Corentin Ravoux, Graziano Rossi, Donald P. Schneider, Hee-Jong Seo, Anže Slosar, Julianna Stermer, M. Vivek, Christophe Yèche, and Samantha Youles. "The Completed SDSS-IV Extended Baryon Oscillation Spectroscopic Survey: Baryon Acoustic Oscillations with Ly$\upalpha$ Forests". In: *The Astrophysical Journal* 901.2 (2020), p. 153. DOI: 10.3847/1538-4357/abb085 (cit. on p. 31).

[dMas+17] Hélion du Mas des Bourboux, Jean-Marc Le Goff, Michael Blomqvist, Nicolás G. Busca, Julien Guy, James Rich, Christophe Yèche, Julian E. Bautista, Étienne Burtin, Kyle S. Dawson, Daniel J. Eisenstein, Andreu Font-Ribera, David Kirkby, Jordi Miralda-Escudé, Pasquier Noterdaeme, Nathalie Palanque-Delabrouille, Isabelle Pâris, Patrick Petitjean, Ignasi Pérez-Ràfols, Matthew M. Pieri, Nicholas P. Ross, David J. Schlegel, Donald P. Schneider, Anže Slosar, David H. Weinberg, and Pauline Zarrouk. "Baryon Acoustic Oscillations from the Complete SDSS-III Lyα-Quasar Cross-Correlation Function at z = 2.4". In: *Astronomy and Astrophysics* 608 (1, 2017), A130. DOI: 10.1051/0004-6361/201731731 (cit. on p. 31).

[Dut+21] D. Dutcher et al. "Measurements of the E-Mode Polarization and Temperature-E-Mode Correlation of the CMB from SPT-3G 2018 Data". In: *Physical Review D* 104.2 (13, 2021), p. 022003. DOI: 10.1103/PhysRevD.104.022003 (cit. on p. 21).

[ESM90] G. Efstathiou, W. J. Sutherland, and S. J. Maddox. "The Cosmological Constant and Cold Dark Matter". In: *Nature* 348 (1, 1990), pp. 705–707. DOI: 10.1038/348705a0 (cit. on p. 9).

[Eis+11] Daniel J. Eisenstein, David H. Weinberg, et al. "SDSS-III: Massive Spectroscopic Surveys of the Distant Universe, the Milky Way, and Extra-Solar Planetary Systems". In: *The Astronomical Journal* 142 (1, 2011), p. 72. DOI: 10.1088/0004-6256/142/3/72; (cit. on p. 20).

[Eis+05] Daniel J. Eisenstein, Idit Zehavi, David W. Hogg, Roman Scoccimarro, Michael R. Blanton, Robert C. Nichol, Ryan Scranton, Hee-Jong Seo, Max Tegmark, Zheng Zheng, Scott F. Anderson, Jim Annis, Neta Bahcall, Jon Brinkmann, Scott Burles, Francisco J. Castander, Andrew Connolly, Istvan Csabai, Mamoru Doi, Masataka Fukugita, Joshua A. Frieman, Karl Glazebrook, James E. Gunn, John S. Hendry, Gregory Hennessy, Zeljko Ivezić, Stephen Kent, Gillian R. Knapp, Huan Lin, Yeong-Shang Loh, Robert H. Lupton, Bruce Margon, Timothy A. McKay, Avery Meiksin, Jeffery A. Munn, Adrian Pope, Michael W. Richmond, David Schlegel, Donald P. Schneider, Kazuhiro Shimasaku, Christopher Stoughton, Michael A. Strauss, Mark SubbaRao, Alexander S. Szalay, István Szapudi, Douglas L. Tucker, Brian Yanny, and Donald G. York. "Detection of the Baryon Acoustic Peak in the Large-Scale Correlation Function of SDSS Luminous Red Galaxies". In: *The Astrophysical Journal* 633.2 (2005), p. 560. DOI: 10.1086/466512 (cit. on p. 10).

[Fau+08] Claude-André Faucher-Giguère, Jason X. Prochaska, Adam Lidz, Lars Hernquist, and Matias Zaldarriaga. "A Direct Precision Measurement of the Intergalactic Lyα Opacity at 2 <= z <= 4.2". In: *The Astrophysical Journal* 681 (1, 2008), pp. 831–855. DOI: 10.1086/588648 (cit. on p. 32).

[Fix09] D. J. Fixsen. “The Temperature of the Cosmic Microwave Background”. In: *The Astrophysical Journal* 707 (1, 2009), pp. 916–920. DOI: 10.1088/0004-637X/707/2/916 (cit. on p. 20).

[Fon+14] Andreu Font-Ribera, David Kirkby, Nicolas Busca, Jordi Miralda-Escudé, Nicholas P. Ross, Anže Slosar, James Rich, Éric Aubourg, Stephen Bailey, Vaishali Bhardwaj, Julian Bautista, Florian Beutler, Dmitry Bizyaev, Michael Blomqvist, Howard Brewington, Jon Brinkmann, Joel R. Brownstein, Bill Carithers, Kyle S. Dawson, Timothée Delubac, Garrett Ebelke, Daniel J. Eisenstein, Jian Ge, Karen Kinemuchi, Khee-Gan Lee, Viktor Malanushenko, Elena Malanushenko, Moses Marchante, Daniel Margala, Demitri Muna, Adam D. Myers, Pasquier Noterdaeme, Daniel Oravetz, Nathalie Palanque-Delabrouille, Isabelle Pâris, Patrick Petitjean, Matthew M. Pieri, Graziano Rossi, Donald P. Schneider, Audrey Simmons, Matteo Viel, Christophe Yeche, and Donald G. York. “Quasar-Lyman-α Forest Cross-Correlation from BOSS DR11: Baryon Acoustic Oscillations”. In: *Journal of Cosmology and Astro-Particle Physics* 05 (1, 2014), p. 027. DOI: 10.1088/1475-7516/2014/05/027 (cit. on p. 31).

[Fon+12] Andreu Font-Ribera, Jordi Miralda-Escudé, Eduard Arnau, Bill Carithers, Khee-Gan Lee, Pasquier Noterdaeme, Isabelle Pâris, Patrick Petitjean, James Rich, Emmanuel Rollinde, Nicholas P. Ross, Donald P. Schneider, Martin White, and Donald G. York. “The Large-Scale Cross-Correlation of Damped Lyman Alpha Systems with the Lyman Alpha Forest: First Measurements from BOSS”. In: *Journal of Cosmology and Astroparticle Physics* 2012.11 (28, 2012), pp. 059–059. DOI: 10.1088/1475-7516/2012/11/059 (cit. on p. 33).

[Fre+19] Wendy L. Freedman, Barry F. Madore, Dylan Hatt, Taylor J. Hoyt, In-Sung Jang, Rachael L. Beaton, Christopher R. Burns, Myung Gyoon Lee, Andrew J. Monson, Jillian R. Neeley, Mark M. Phillips, Jeffrey A. Rich, and Mark Seibert. “The Carnegie-Chicago Hubble Program. VIII. An Independent Determination of the Hubble Constant Based on the Tip of the Red Giant Branch”. In: *The Astrophysical Journal* 882.1 (29, 2019), p. 34. DOI: 10.3847/1538-4357/ab2f73 (cit. on p. 17).

[Gil+20] Héctor Gil-Marín, Julián E. Bautista, Romain Paviot, Mariana Vargas-Magaña, Sylvain de la Torre, Sebastien Fromenteau, Shadab Alam, Santiago Ávila, Etienne Burtin, Chia-Hsun Chuang, Kyle S. Dawson, Jiamin Hou, Arnaud de Mattia, Faizan G. Mohammad, Eva-Maria Müller, Seshadri Nadathur, Richard Neveux, Will J. Percival, Anand Raichoor, Mehdi Rezaie, Ashley J. Ross, Graziano Rossi, Vanina Ruhlmann-Kleider, Alex Smith, Amélie Tamone, Jeremy L. Tinker, Rita Tojeiro, Yuting Wang, Gong-Bo Zhao, Cheng Zhao, Jonathan Brinkmann, Joel R. Brownstein, Peter D. Choi, Stephanie Escoffier, Axel de la Macorra, Jeongin Moon, Jeffrey A. Newman, Donald P. Schneider, Hee-Jong Seo, and Mariappan Vivek. “The Completed SDSS-IV Extended Baryon Oscillation Spectroscopic Survey: Measurement of the BAO and Growth Rate of Structure of the Luminous Red Galaxy Sample from the Anisotropic Power Spectrum between Redshifts 0.6 and 1.0”. In: *Monthly Notices of the Royal Astronomical Society* 498 (1, 2020), pp. 2492–2531. DOI: 10.1093/mnras/staa2455 (cit. on p. 22).

[Gra+19] Matthew J. Graham et al. “The Zwicky Transient Facility: Science Objectives”. In: *Publications of the Astronomical Society of the Pacific* 131 (1, 2019), p. 078001. DOI: 10.1088/1538-3873/ab006c (cit. on p. 18).

[Gra+20] R. Graziani, M. Rigault, N. Regnault, Ph Gris, A. Möller, P. Antilogus, P. Astier, M. Betoule, S. Bongard, M. Briday, J. Cohen-Tanugi, Y. Copin, H. M. Courtois, D. Fouchez, E. Gangler, D. Guinet, A. J. Hawken, Y.-L. Kim, P.-F. Léget, J. Neveu, P. Ntelis, Ph Rosnet, and E. Nuss. "Peculiar Velocity Cosmology with Type Ia Supernovae". 24, 2020 (cit. on p. 18).

[Gun+98] J. E. Gunn, M. Carr, C. Rockosi, M. Sekiguchi, K. Berry, B. Elms, E. de Haas, Ž . Ivezić, G. Knapp, R. Lupton, G. Pauls, R. Simcoe, R. Hirsch, D. Sanford, S. Wang, D. York, F. Harris, J. Annis, L. Bartozek, W. Boroski, J. Bakken, M. Haldeman, S. Kent, S. Holm, D. Holmgren, D. Petravick, A. Prosapio, R. Rechenmacher, M. Doi, M. Fukugita, K. Shimasaku, N. Okada, C. Hull, W. Siegmund, E. Mannery, M. Blouke, D. Heidtman, D. Schneider, R. Lucinio, and J. Brinkman. "The Sloan Digital Sky Survey Photometric Camera". In: *The Astronomical Journal* 116 (1, 1998), pp. 3040–3081. DOI: 10.1086/300645 (cit. on p. 24).

[GP65] James E. Gunn and Bruce A. Peterson. "On the Density of Neutral Hydrogen in Intergalactic Space." In: *The Astrophysical Journal* 142 (1, 1965), pp. 1633–1641. DOI: 10.1086/148444 (cit. on p. 30).

[Her+99] J. R. Herrnstein, J. M. Moran, L. J. Greenhill, P. J. Diamond, M. Inoue, N. Nakai, M. Miyoshi, C. Henkel, and A. Riess. "A Geometric Distance to the Galaxy NGC4258 from Orbital Motions in a Nuclear Gas Disk". In: *Nature* 400.6744 (6744 1999), pp. 539–541. DOI: 10.1038/22972 (cit. on p. 17).

[Hey+21] Catherine Heymans, Tilman Tröster, Marika Asgari, Chris Blake, Hendrik Hildebrandt, Benjamin Joachimi, Konrad Kuijken, Chieh-An Lin, Ariel G. Sánchez, Jan Luca van den Busch, Angus H. Wright, Alexandra Amon, Maciej Bilicki, Jelte de Jong, Martin Crocce, Andrej Dvornik, Thomas Erben, Maria Cristina Fortuna, Fedor Getman, Benjamin Giblin, Karl Glazebrook, Henk Hoekstra, Shahab Joudaki, Arun Kannawadi, Fabian Köhlinger, Chris Lidman, Lance Miller, Nicola R. Napolitano, David Parkinson, Peter Schneider, HuanYuan Shan, Edwin Valentijn, Gijs Verdoes Kleijn, and Christian Wolf. "KiDS-1000 Cosmology: Multi-probe Weak Gravitational Lensing and Spectroscopic Galaxy Clustering Constraints". In: *Astronomy & Astrophysics* 646 (2021), A140. DOI: 10.1051/0004-6361/202039063 (cit. on p. 23).

[Hik+19] Chiaki Hikage, Masamune Oguri, Takashi Hamana, Surhud More, Rachel Mandelbaum, Masahiro Takada, Fabian Köhlinger, Hironao Miyatake, Atsushi J. Nishizawa, Hiroaki Aihara, Robert Armstrong, James Bosch, Jean Coupon, Anne Ducout, Paul Ho, Bau-Ching Hsieh, Yutaka Komiyama, François Lanusse, Alexie Leauthaud, Robert H. Lupton, Elinor Medezinski, Sogo Mineo, Shoken Miyama, Satoshi Miyazaki, Ryoma Murata, Hitoshi Murayama, Masato Shirasaki, Cristóbal Sifón, Melanie Simet, Joshua Speagle, David N. Spergel, Michael A. Strauss, Naoshi Sugiyama, Masayuki Tanaka, Yousuke Utsumi, Shiang-Yu Wang, and Yoshihiko Yamada. "Cosmology from Cosmic Shear Power Spectra with Subaru Hyper Suprime-Cam First-Year Data". In: *Publications of the Astronomical Society of Japan* 71 (1, 2019), p. 43. DOI: 10.1093/pasj/psz010 (cit. on p. 23).

[Hor86] K. Horne. "An Optimal Extraction Algorithm for CCD Spectroscopy." In: *Publications of the Astronomical Society of the Pacific* 98 (1, 1986), pp. 609–617. DOI: 10.1086/131801 (cit. on p. 27).

[Hou+21] Jiamin Hou, Ariel G. Sánchez, Ashley J. Ross, Alex Smith, Richard Neveux, Julian Bautista, Etienne Burtin, Cheng Zhao, Román Scoccimarro, Kyle S. Dawson, Arnaud de Mattia, Axel de la Macorra, Hélion du Mas des Bourboux, Daniel J. Eisenstein, Héctor Gil-Marín, Brad W. Lyke, Faizan G. Mohammad, Eva-Maria Mueller, Will J. Percival, Graziano Rossi, Mariana Vargas Magaña, Pauline Zarrouk, Gong-Bo Zhao, Jonathan Brinkmann, Joel R. Brownstein, Chia-Hsun Chuang, Adam D. Myers, Jeffrey A. Newman, Donald P. Schneider, and M. Vivek. "The Completed SDSS-IV Extended Baryon Oscillation Spectroscopic Survey: BAO and RSD Measurements from Anisotropic Clustering Analysis of the Quasar Sample in Configuration Space between Redshift 0.8 and 2.2". In: *Monthly Notices of the Royal Astronomical Society* 500 (1, 2021), pp. 1201–1221. DOI: 10.1093/mnras/staa3234 (cit. on p. 22).

[How+15] Cullan Howlett, Ashley J. Ross, Lado Samushia, Will J. Percival, and Marc Manera. "The Clustering of the SDSS Main Galaxy Sample - II. Mock Galaxy Catalogues and a Measurement of the Growth of Structure from Redshift Space Distortions at z = 0.15". In: *Monthly Notices of the Royal Astronomical Society* 449 (1, 2015), pp. 848–866. DOI: 10.1093/mnras/stu2693 (cit. on p. 22).

[Hub29] Edwin Hubble. "A Relation between Distance and Radial Velocity among Extra-Galactic Nebulae". In: *Proceedings of the National Academy of Sciences* 15.3 (15, 1929), pp. 168–173. DOI: 10.1073/pnas.15.3.168 (cit. on p. 16).

[Kai87] Nick Kaiser. "Clustering in Real Space and in Redshift Space". In: *Monthly Notices of the Royal Astronomical Society* 227 (1, 1987), pp. 1–21. DOI: 10.1093/mnras/227.1.1 (cit. on p. 22).

[Kam+20] Vikrant Kamble, Kyle Dawson, Hélion du Mas des Bourboux, Julian Bautista, and Donald P. Scheinder. "Measurements of Effective Optical Depth in the Lyα Forest from the BOSS DR12 Quasar Sample". In: *The Astrophysical Journal* 892 (1, 2020), p. 70. DOI: 10.3847/1538-4357/ab76bd (cit. on p. 32).

[Kes+19] R Kessler et al. "First Cosmology Results Using Type Ia Supernova from the Dark Energy Survey: Simulations to Correct Supernova Distance Biases". In: *Monthly Notices of the Royal Astronomical Society* 485.1 (1, 2019), pp. 1171–1187. DOI: 10.1093/mnras/stz463 (cit. on p. 18).

[KL20] Alex G. Kim and Eric V. Linder. "Complementarity of Peculiar Velocity Surveys and Redshift Space Distortions for Testing Gravity". In: *Physical Review D* 101 (1, 2020), p. 023516. DOI: 10.1103/PhysRevD.101.023516 (cit. on p. 18).

[Kir+13] David Kirkby, Daniel Margala, Anže Slosar, Stephen Bailey, Nicolás G. Busca, Timothée Delubac, James Rich, Julian E. Bautista, Michael Blomqvist, Joel R. Brownstein, Bill Carithers, Rupert A. C. Croft, Kyle S. Dawson, Andreu Font-Ribera, Jordi Miralda-Escudé, Adam D. Myers, Robert C. Nichol, Nathalie Palanque-Delabrouille, Isabelle Pâris, Patrick Petitjean, Graziano Rossi, David J. Schlegel, Donald P. Schneider, Matteo Viel, David H. Weinberg, and Christophe Yèche. "Fitting Methods for Baryon Acoustic Oscillations in the Lyman-α Forest Fluctuations in BOSS Data Release 9". In: *Journal of Cosmology and Astro-Particle Physics* 2013.3 (2013), p. 024. DOI: 10.1088/1475-7516/2013/03/024 (cit. on p. 31).

[LSS12] Khee-Gan Lee, Nao Suzuki, and David N. Spergel. “Mean-Flux-Regulated Principal Component Analysis Continuum Fitting of Sloan Digital Sky Survey Lyα Forest Spectra”. In: *The Astronomical Journal* 143 (1, 2012), p. 51. DOI: 10.1088/0004-6256/143/2/51 (cit. on p. 32).

[Les11] Julien Lesgourgues. “The Cosmic Linear Anisotropy Solving System (CLASS) I: Overview”. In: (14, 2011) (cit. on p. 21).

[LCL00] Antony Lewis, Anthony Challinor, and Anthony Lasenby. “Efficient Computation of Cosmic Microwave Background Anisotropies in Closed Friedmann-Robertson-Walker Models”. In: *The Astrophysical Journal* 538 (1, 2000), pp. 473–476. DOI: 10.1086/309179 (cit. on p. 21).

[Lin03] Eric V. Linder. “Exploring the Expansion History of the Universe”. In: *Physical Review Letters* 90 (1, 2003), p. 091301. DOI: 10.1103/PhysRevLett.90.091301 (cit. on p. 12).

[Lup+01] R. Lupton, J. E. Gunn, Z. Ivezić, G. R. Knapp, and S. Kent. “The SDSS Imaging Pipelines”. In: 238 (1, 2001), p. 269 (cit. on p. 24).

[Mad+90] S. J. Maddox, G. Efstathiou, W. J. Sutherland, and J. Loveday. “Galaxy Correlations on Large Scales.” In: *Monthly Notices of the Royal Astronomical Society* 242 (1, 1990), p. 43. DOI: 10.1093/mnras/242.1.43P (cit. on p. 9).

[Mat+94] J. C. Mather, E. S. Cheng, D. A. Cottingham, R. E. Eplee Jr., D. J. Fixsen, T. Hewagama, R. B. Isaacman, K. A. Jensen, S. S. Meyer, P. D. Noerdlinger, S. M. Read, L. P. Rosen, R. A. Shafer, E. L. Wright, C. L. Bennett, N. W. Boggess, M. G. Hauser, T. Kelsall, S. H. Moseley Jr., R. F. Silverberg, G. F. Smoot, R. Weiss, and D. T. Wilkinson. “Measurement of the Cosmic Microwave Background Spectrum by the COBE FIRAS Instrument”. In: *The Astrophysical Journal* 420 (1, 1994), pp. 439–444. DOI: 10.1086/173574 (cit. on p. 20).

[McD03] Patrick McDonald. “Toward a Measurement of the Cosmological Geometry at \$z \sim 2\$: Predicting Ly\$\alpha\$ Forest Correlation in Three Dimensions and the Potential of Future Data Sets”. In: *The Astrophysical Journal* 585 (1, 2003), pp. 34–51. DOI: 10.1086/345945 (cit. on p. 30).

[McD+00] Patrick McDonald, Jordi Miralda-Escudé, Michael Rauch, Wallace L. W. Sargent, Tom A. Barlow, Renyue Cen, and Jeremiah P. Ostriker. “The Observed Probability Distribution Function, Power Spectrum, and Correlation Function of the Transmitted Flux in the Ly\$\alpha\$ Forest”. In: *The Astrophysical Journal* 543 (1, 2000), pp. 1–23. DOI: 10.1086/317079 (cit. on p. 30).

[McD+06] Patrick McDonald, Uroš Seljak, Scott Burles, David J. Schlegel, David H. Weinberg, Renyue Cen, David Shih, Joop Schaye, Donald P. Schneider, Neta A. Bahcall, John W. Briggs, J. Brinkmann, Robert J. Brunner, Masataka Fukugita, James E. Gunn, Željko Ivezić, Stephen Kent, Robert H. Lupton, and Daniel E. Vanden Berk. “The Ly\$\alpha\$ Forest Power Spectrum from the Sloan Digital Sky Survey”. In: *The Astrophysical Journal Supplement Series* 163 (1, 2006), pp. 80–109. DOI: 10.1086/444361; (cit. on p. 30).

[McD+05] Patrick McDonald, Uroš Seljak, Renyue Cen, David Shih, David H. Weinberg, Scott Burles, Donald P. Schneider, David J. Schlegel, Neta A. Bahcall, John W. Briggs, J. Brinkmann, Masataka Fukugita, Željko Ivezić, Stephen Kent, and Daniel E. Vanden Berk. "The Linear Theory Power Spectrum from the Lyα Forest in the Sloan Digital Sky Survey". In: *The Astrophysical Journal* 635 (1, 2005), pp. 761–783. DOI: 10.1086/497563 (cit. on p. 30).

[Mou+00] Jeremy R. Mould, John P. Huchra, Wendy L. Freedman, Robert C. Kennicutt Jr., Laura Ferrarese, Holland C. Ford, Brad K. Gibson, John A. Graham, Shaun M. G. Hughes, Garth D. Illingworth, Daniel D. Kelson, Lucas M. Macri, Barry F. Madore, Shoko Sakai, Kim M. Sebo, Nancy A. Silbermann, and Peter B. Stetson. "The Hubble Space Telescope Key Project on the Extragalactic Distance Scale. XXVIII. Combining the Constraints on the Hubble Constant". In: *The Astrophysical Journal* 529 (1, 2000), pp. 786–794. DOI: 10.1086/308304 (cit. on p. 9).

[Mye+15] Adam D. Myers, Nathalie Palanque-Delabrouille, Abhishek Prakash, Isabelle Pâris, Christophe Yeche, Kyle S. Dawson, Jo Bovy, Dustin Lang, David J. Schlegel, Jeffrey A. Newman, Patrick Petitjean, Jean Paul Kneib, Pierre Laurent, Will J. Percival, Ashley J. Ross, Hee-Jong Seo, Jeremy L. Tinker, Eric Armengaud, Joel Brownstein, Etienne Burtin, Zheng Cai, Johan Comparat, Mansi Kasliwal, Shrinivas R. Kulkarni, Russ Laher, David Levitan, Cameron K. McBride, Ian D. McGreer, Adam A. Miller, Peter Nugent, Eran Ofek, Graziano Rossi, John Ruan, Donald P. Schneider, Branimir Sesar, Alina Streblyanska, Jason Surace, and for the SDSS-IV/eBOSS collaboration. "The SDSS-IV Extended Baryon Oscillation Spectroscopic Survey: Quasar Target Selection". In: *The Astrophysical Journal Supplement Series* 221.2 (2, 2015), p. 27. DOI: 10.1088/0067-0049/221/2/27 (cit. on p. 25).

[Nev+20] Richard Neveux, Etienne Burtin, Arnaud de Mattia, Alex Smith, Ashley J. Ross, Jiamin Hou, Julian Bautista, Jonathan Brinkmann, Chia-Hsun Chuang, Kyle S. Dawson, Héctor Gil-Marín, Brad W. Lyke, Axel de la Macorra, Hélion du Mas des Bourboux, Faizan G. Mohammad, Eva-Maria Müller, Adam D. Myers, Jeffrey A. Newman, Will J. Percival, Graziano Rossi, Donald Schneider, M. Vivek, Pauline Zarrouk, Cheng Zhao, and Gong-Bo Zhao. "The Completed SDSS-IV Extended Baryon Oscillation Spectroscopic Survey: BAO and RSD Measurements from the Anisotropic Power Spectrum of the Quasar Sample between Redshift 0.8 and 2.2". In: *Monthly Notices of the Royal Astronomical Society* 499 (1, 2020), pp. 210–229. DOI: 10.1093/mnras/staa2780 (cit. on p. 22).

[Oku+16] Teppei Okumura, Chiaki Hikage, Tomonori Totani, Motonari Tonegawa, Hiroyuki Okada, Karl Glazebrook, Chris Blake, Pedro G. Ferreira, Surhud More, Atsushi Taruya, Shinji Tsujikawa, Masayuki Akiyama, Gavin Dalton, Tomotsugu Goto, Takashi Ishikawa, Fumihide Iwamuro, Takahiko Matsubara, Takahiro Nishimichi, Kouji Ohta, Ikkoh Shimizu, Ryuichi Takahashi, Naruhisa Takato, Naoyuki Tamura, Kiyoto Yabe, and Naoki Yoshida. "The Subaru FMOS Galaxy Redshift Survey (FastSound). IV. New Constraint on Gravity Theory from Redshift Space Distortions at z \sim 1.4". In: *Publications of the Astronomical Society of Japan* 68.3 (1, 2016). DOI: 10.1093/pasj/psw029 (cit. on p. 20).

[Pad+08] Nikhil Padmanabhan, David J. Schlegel, Douglas P. Finkbeiner, J. C. Barentine, Michael R. Blanton, Howard J. Brewington, James E. Gunn, Michael Harvanek, David W. Hogg, Željko Ivezić, David Johnston, Stephen M. Kent, S. J. Kleinman, Gillian R. Knapp, Jurek Krzesinski, Dan Long, Eric H. Neilsen Jr., Atsuko Nitta, Craig Loomis, Robert H. Lupton, Sam Roweis, Stephanie A. Snedden, Michael A. Strauss, and Douglas L. Tucker. "An Improved Photometric Calibration of the Sloan Digital Sky Survey Imaging Data". In: *The Astrophysical Journal* 674 (1, 2008), pp. 1217–1233. DOI: 10.1086/524677 (cit. on p. 24).

[Pal+16] N. Palanque-Delabrouille, Ch. Magneville, Ch. Yèche, I. Pâris, P. Petitjean, E. Burtin, K. Dawson, I. McGreer, A. D. Myers, G. Rossi, D. Schlegel, D. Schneider, A. Streblyanska, and J. Tinker. "The Extended Baryon Oscillation Spectroscopic Survey: Variability Selection and Quasar Luminosity Function". In: *Astronomy and Astrophysics* 587 (1, 2016), A41. DOI: 10.1051/0004-6361/201527392 (cit. on p. 25).

[Pal+20] Nathalie Palanque-Delabrouille, Christophe Yèche, Nils Schöneberg, Julien Lesgourgues, Michael Walther, Solène Chabanier, and Eric Armengaud. "Hints, Neutrino Bounds, and WDM Constraints from SDSS DR14 Lyman-$\upalpha$ and Planck Full-Survey Data". In: *Journal of Cosmology and Astroparticle Physics* 2020.04 (2020), pp. 038–038. DOI: 10.1088/1475-7516/2020/04/038 (cit. on p. 30).

[Pâr+11] I. Pâris, P. Petitjean, E. Rollinde, E. Aubourg, N. Busca, R. Charlassier, T. Delubac, J.-Ch Hamilton, J.-M. Le Goff, N. Palanque-Delabrouille, S. Peirani, Ch Pichon, J. Rich, M. Vargas-Magaña, and Ch Yèche. "A Principal Component Analysis of Quasar UV Spectra at z ~ 3". In: *Astronomy and Astrophysics* 530 (2011), A50. DOI: 10.1051/0004-6361/201016233 (cit. on p. 32).

[Par+12] David Parkinson, Signe Riemer-Sørensen, Chris Blake, Gregory B. Poole, Tamara M. Davis, Sarah Brough, Matthew Colless, Carlos Contreras, Warrick Couch, Scott Croom, Darren Croton, Michael J. Drinkwater, Karl Forster, David Gilbank, Mike Gladders, Karl Glazebrook, Ben Jelliffe, Russell J. Jurek, I.-hui Li, Barry Madore, D. Christopher Martin, Kevin Pimbblet, Michael Pracy, Rob Sharp, Emily Wisnioski, David Woods, Ted K. Wyder, and H. K. C. Yee. "The WiggleZ Dark Energy Survey: Final Data Release and Cosmological Results". In: *Physical Review D* 86.10 (2012), p. 103518. DOI: 10.1103/PhysRevD.86.103518 (cit. on p. 20).

[Per+99] S. Perlmutter, G. Aldering, G. Goldhaber, R. A. Knop, P. Nugent, P. G. Castro, S. Deustua, S. Fabbro, A. Goobar, D. E. Groom, I. M. Hook, A. G. Kim, M. Y. Kim, J. C. Lee, N. J. Nunes, R. Pain, C. R. Pennypacker, R. Quimby, C. Lidman, R. S. Ellis, M. Irwin, R. G. McMahon, P. Ruiz-Lapuente, N. Walton, B. Schaefer, B. J. Boyle, A. V. Filippenko, T. Matheson, A. S. Fruchter, N. Panagia, H. J. M. Newberg, W. J. Couch, and Supernova Cosmology Project. "Measurements of Omega and Lambda from 42 High-Redshift Supernovae". In: *The Astrophysical Journal* 517 (1, 1999), pp. 565–586. DOI: 10.1086/307221 (cit. on p. 9).

[Pez+17] A. Pezzotta, S. de la Torre, J. Bel, B. R. Granett, L. Guzzo, J. A. Peacock, B. Garilli, M. Scodeggio, M. Bolzonella, U. Abbas, C. Adami, D. Bottini, A. Cappi, O. Cucciati, I. Davidzon, P. Franzetti, A. Fritz, A. Iovino, J. Krywult, V. Le Brun, O. Le Fèvre, D. Maccagni, K. Małek, F. Marulli, M. Polletta, A. Pollo, L. a. M. Tasca, R. Tojeiro, D. Vergani, A. Zanichelli, S. Arnouts, E. Branchini, J. Coupon, G. De Lucia, J. Koda, O. Ilbert, F. Mohammad, T. Moutard, and L. Moscardini. "The VIMOS Public Extragalactic Redshift Survey (VIPERS). The Growth of Structure at 0.5 < z < 1.2 from Redshift-Space Distortions in the Clustering of the PDR-2 Final

Sample". In: *Astronomy and Astrophysics* 604 (2017), A33. DOI: 10.1051/0004-6361/201630295 (cit. on p. 20).

[Pit+21] Cyril Pitrou, Alain Coc, Jean-Philippe Uzan, and Elisabeth Vangioni. "A New Tension in the Cosmological Model from Primordial Deuterium?" In: *Monthly Notices of the Royal Astronomical Society* 502.2 (10, 2021), pp. 2474–2481. DOI: 10.1093/mnras/stab135 (cit. on p. 19).

[Pla+20] Planck Collaboration et al. "Planck 2018 Results. VI. Cosmological Parameters". In: *Astronomy and Astrophysics* 641 (1, 2020), A6. DOI: 10.1051/0004-6361/201833910 (cit. on p. 21).

[Pra+16] Abhishek Prakash, Timothy C. Licquia, Jeffrey A. Newman, Ashley J. Ross, Adam D. Myers, Kyle S. Dawson, Jean-Paul Kneib, Will J. Percival, Julian E. Bautista, Johan Comparat, Jeremy L. Tinker, David J. Schlegel, Rita Tojeiro, Shirley Ho, Dustin Lang, Sandhya M. Rao, Cameron K. McBride, Guangtun Ben Zhu, Joel R. Brownstein, Stephen Bailey, Adam S. Bolton, Timothée Delubac, Vivek Mariappan, Michael R. Blanton, Beth Reid, Donald P. Schneider, Hee-Jong Seo, Aurelio Carnero Rosell, and Francisco Prada. "The SDSS-IV Extended Baryon Oscillation Spectroscopic Survey: Luminous Red Galaxy Target Selection". In: *The Astrophysical Journal Supplement Series* 224 (1, 2016), p. 34. DOI: 10.3847/0067-0049/224/2/34 (cit. on p. 25).

[Rai+17] A. Raichoor, J. Comparat, T. Delubac, J.-P. Kneib, Ch Yèche, K. S. Dawson, W. J. Percival, A. Dey, D. Lang, D. J. Schlegel, C. Gorgoni, J. Bautista, J. R. Brownstein, V. Mariappan, H.-J. Seo, J. L. Tinker, A. J. Ross, Y. Wang, G.-B. Zhao, J. Moustakas, N. Palanque-Delabrouille, E. Jullo, J. A. Newmann, F. Prada, and G. B. Zhu. "The SDSS-IV Extended Baryon Oscillation Spectroscopic Survey: Final Emission Line Galaxy Target Selection". In: *Monthly Notices of the Royal Astronomical Society* 471 (1, 2017), pp. 3955–3973. DOI: 10.1093/mnras/stx1790 (cit. on p. 25).

[Rei+16] Beth Reid, Shirley Ho, Nikhil Padmanabhan, Will J. Percival, Jeremy Tinker, Rita Tojeiro, Martin White, Daniel J. Eisenstein, Claudia Maraston, Ashley J. Ross, Ariel G. Sánchez, David Schlegel, Erin Sheldon, Michael A. Strauss, Daniel Thomas, David Wake, Florian Beutler, Dmitry Bizyaev, Adam S. Bolton, Joel R. Brownstein, Chia-Hsun Chuang, Kyle Dawson, Paul Harding, Francisco-Shu Kitaura, Alexie Leauthaud, Karen Masters, Cameron K. McBride, Surhud More, Matthew D. Olmstead, Daniel Oravetz, Sebastián E. Nuza, Kaike Pan, John Parejko, Janine Pforr, Francisco Prada, Sergio Rodríguez-Torres, Salvador Salazar-Albornoz, Lado Samushia, Donald P. Schneider, Claudia G. Scóccola, Audrey Simmons, and Mariana Vargas-Magana. "SDSS-III Baryon Oscillation Spectroscopic Survey Data Release 12: Galaxy Target Selection and Large-Scale Structure Catalogues". In: *Monthly Notices of the Royal Astronomical Society* 455 (1, 2016), pp. 1553–1573. DOI: 10.1093/mnras/stv2382 (cit. on p. 25).

[RPR19] M. J. Reid, D. W. Pesce, and A. G. Riess. "An Improved Distance to NGC 4258 and Its Implications for the Hubble Constant". In: *The Astrophysical Journal* 886.2 (2019), p. L27. DOI: 10.3847/2041-8213/ab552d (cit. on p. 17).

[Rie20] Adam G. Riess. "The Expansion of the Universe Is Faster than Expected". In: *Nature Reviews Physics* 2.1 (2020), pp. 10–12. DOI: 10.1038/s42254-019-0137-0 (cit. on p. 16).

[Rie+21] Adam G. Riess, Stefano Casertano, Wenlong Yuan, J. Bradley Bowers, Lucas Macri, Joel C. Zinn, and Dan Scolnic. “Cosmic Distances Calibrated to 1% Precision with Gaia EDR3 Parallaxes and Hubble Space Telescope Photometry of 75 Milky Way Cepheids Confirm Tension with ${upLambda”. In: 908.1 (2021), p. L6. DOI: 10.3847/2041-8213/abdbaf (cit. on p. 16).

[Rie+98] Adam G. Riess, Alexei V. Filippenko, Peter Challis, Alejandro Clocchiatti, Alan Diercks, Peter M. Garnavich, Ron L. Gilliland, Craig J. Hogan, Saurabh Jha, Robert P. Kirshner, B. Leibundgut, M. M. Phillips, David Reiss, Brian P. Schmidt, Robert A. Schommer, R. Chris Smith, J. Spyromilio, Christopher Stubbs, Nicholas B. Suntzeff, and John Tonry. “Observational Evidence from Supernovae for an Accelerating Universe and a Cosmological Constant”. In: *The Astronomical Journal* 116 (1, 1998), pp. 1009–1038. DOI: 10.1086/300499 (cit. on p. 9).

[Ros+12] Nicholas P. Ross, Adam D. Myers, Erin S. Sheldon, Christophe Yèche, Michael A. Strauss, Jo Bovy, Jessica A. Kirkpatrick, Gordon T. Richards, Éric Aubourg, Michael R. Blanton, W. N. Brandt, William C. Carithers, Rupert A. C. Croft, Robert da Silva, Kyle Dawson, Daniel J. Eisenstein, Joseph F. Hennawi, Shirley Ho, David W. Hogg, Khee-Gan Lee, Britt Lundgren, Richard G. McMahon, Jordi Miralda-Escudé, Nathalie Palanque-Delabrouille, Isabelle Pâris, Patrick Petitjean, Matthew M. Pieri, James Rich, Natalie A. Roe, David Schiminovich, David J. Schlegel, Donald P. Schneider, Anže Slosar, Nao Suzuki, Jeremy L. Tinker, David H. Weinberg, Anya Weyant, Martin White, and W. Michael Wood-Vasey. “The SDSS-III Baryon Oscillation Spectroscopic Survey: Quasar Target Selection for Data Release Nine”. In: *The Astrophysical Journal Supplement Series* 199.1 (2012), p. 3. DOI: 10.1088/0067-0049/199/1/3 (cit. on p. 25).

[Sán20] Ariel G. Sánchez. “Arguments against Using $h\hat{}{-1}$ Mpc Units in Observational Cosmology”. In: *Physical Review D* 102.12 (2, 2020), p. 123511. DOI: 10.1103/PhysRevD.102.123511 (cit. on p. 16).

[Sco+18] D. M. Scolnic, D. O. Jones, A. Rest, Y. C. Pan, R. Chornock, R. J. Foley, M. E. Huber, R. Kessler, G. Narayan, A. G. Riess, S. Rodney, E. Berger, D. J. Brout, P. J. Challis, M. Drout, D. Finkbeiner, R. Lunnan, R. P. Kirshner, N. E. Sanders, E. Schlafly, S. Smartt, C. W. Stubbs, J. Tonry, W. M. Wood-Vasey, M. Foley, J. Hand, E. Johnson, W. S. Burgett, K. C. Chambers, P. W. Draper, K. W. Hodapp, N. Kaiser, R. P. Kudritzki, E. A. Magnier, N. Metcalfe, F. Bresolin, E. Gall, R. Kotak, M. McCrum, and K. W. Smith. “The Complete Light-curve Sample of Spectroscopically Confirmed SNe Ia from Pan-STARRS1 and Cosmological Constraints from the Combined Pantheon Sample”. In: *The Astrophysical Journal* 859 (1, 2018), p. 101. DOI: 10.3847/1538-4357/aab9bb (cit. on p. 18).

[Slo+11] Anže Slosar, Andreu Font-Ribera, Matthew M. Pieri, James Rich, Jean-Marc Le Goff, Éric Aubourg, Jon Brinkmann, Nicolas Busca, Bill Carithers, Romain Charlassier, Marina Cortês, Rupert Croft, Kyle S. Dawson, Daniel Eisenstein, Jean-Christophe Hamilton, Shirley Ho, Khee-Gan Lee, Robert Lupton, Patrick McDonald, Bumbarija Medolin, Demitri Muna, Jordi Miralda-Escudé, Adam D. Myers, Robert C. Nichol, Nathalie Palanque-Delabrouille, Isabelle Pâris, Patrick Petitjean, Yodovina Piškur, Emmanuel Rollinde, Nicholas P. Ross, David J. Schlegel, Donald P. Schneider, Erin Sheldon, Benjamin A. Weaver, David H. Weinberg, Christophe Yeche, and Donald G. York. “The Lyman-α Forest in Three

Dimensions: Measurements of Large Scale Flux Correlations from BOSS 1st-Year Data". In: *Journal of Cosmology and Astroparticle Physics* 2011.9 (2011), p. 001. DOI: 10.1088/1475-7516/2011/09/001 (cit. on p. 31).

[Slo+13] Anže Slosar, Vid Iršič, David Kirkby, Stephen Bailey, Nicolás G. Busca, Timothée Delubac, James Rich, Éric Aubourg, Julian E. Bautista, Vaishali Bhardwaj, Michael Blomqvist, Adam S. Bolton, Jo Bovy, Joel Brownstein, Bill Carithers, Rupert A. C. Croft, Kyle S. Dawson, Andreu Font-Ribera, J.-M. Le Goff, Shirley Ho, Klaus Honscheid, Khee-Gan Lee, Daniel Margala, Patrick McDonald, Bumbarija Medolin, Jordi Miralda-Escudé, Adam D. Myers, Robert C. Nichol, Pasquier Noterdaeme, Nathalie Palanque-Delabrouille, Isabelle Pâris, Patrick Petitjean, Matthew M. Pieri, Yodovina Piškur, Natalie A. Roe, Nicholas P. Ross, Graziano Rossi, David J. Schlegel, Donald P. Schneider, Nao Suzuki, Erin S. Sheldon, Uroš Seljak, Matteo Viel, David H. Weinberg, and Christophe Yèche. "Measurement of Baryon Acoustic Oscillations in the Lyman-α Forest Fluctuations in BOSS Data Release 9". In: *Journal of Cosmology and Astro-Particle Physics* 04 (1, 2013), p. 026. DOI: 10.1088/1475-7516/2013/04/026; (cit. on p. 31).

[Str+02] Michael A. Strauss, David H. Weinberg, Robert H. Lupton, Vijay K. Narayanan, James Annis, Mariangela Bernardi, Michael Blanton, Scott Burles, A. J. Connolly, Julianne Dalcanton, Mamoru Doi, Daniel Eisenstein, Joshua A. Frieman, Masataka Fukugita, James E. Gunn, Željko Ivezić, Stephen Kent, Rita S. J. Kim, G. R. Knapp, Richard G. Kron, Jeffrey A. Munn, Heidi Jo Newberg, R. C. Nichol, Sadanori Okamura, Thomas R. Quinn, Michael W. Richmond, David J. Schlegel, Kazuhiro Shimasaku, Mark SubbaRao, Alexander S. Szalay, Dan Vanden Berk, Michael S. Vogeley, Brian Yanny, Naoki Yasuda, Donald G. York, and Idit Zehavi. "Spectroscopic Target Selection in the Sloan Digital Sky Survey: The Main Galaxy Sample". In: *The Astronomical Journal* 124 (1, 2002), pp. 1810–1824. DOI: 10.1086/342343 (cit. on p. 25).

[Tam+20] Amélie Tamone, Anand Raichoor, Cheng Zhao, Arnaud de Mattia, Claudio Gorgoni, Etienne Burtin, Vanina Ruhlmann-Kleider, Ashley J. Ross, Shadab Alam, Will J. Percival, Santiago Avila, Michael J. Chapman, Chia-Hsun Chuang, Johan Comparat, Kyle S. Dawson, Sylvain de la Torre, Hélion du Mas des Bourboux, Stephanie Escoffier, Violeta Gonzalez-Perez, Jiamin Hou, Jean-Paul Kneib, Faizan G. Mohammad, Eva-Maria Mueller, Romain Paviot, Graziano Rossi, Donald P. Schneider, Yuting Wang, and Gong-Bo Zhao. "The Completed SDSS-IV Extended Baryon Oscillation Spectroscopic Survey: Growth Rate of Structure Measurement from Anisotropic Clustering Analysis in Configuration Space between Redshift 0.6 and 1.1 for the Emission Line Galaxy Sample". In: *Monthly Notices of the Royal Astronomical Society* (1, 2020). DOI: 10.1093/mnras/staa3050 (cit. on p. 22).

[Wei+13] David H. Weinberg, Michael J. Mortonson, Daniel J. Eisenstein, Christopher Hirata, Adam G. Riess, and Eduardo Rozo. "Observational Probes of Cosmic Acceleration". In: *Physics Reports* 530.2 (10, 2013), pp. 87–255. DOI: 10.1016/j.physrep.2013.05.001 (cit. on p. 12).

[Won+19] Kenneth C. Wong, Sherry H. Suyu, Geoff C.-F. Chen, Cristian E. Rusu, Martin Millon, Dominique Sluse, Vivien Bonvin, Christopher D. Fassnacht, Stefan Taubenberger, Matthew W. Auger, Simon Birrer, James H. H. Chan, Frederic Courbin, Stefan Hilbert, Olga Tihhonova, Tommaso Treu, Adriano Agnello, Xuheng Ding, Inh

Jee, Eiichiro Komatsu, Anowar J. Shajib, Alessandro Sonnenfeld, Roger D. Blandford, Léon V. E. Koopmans, Philip J. Marshall, and Georges Meylan. "H0LiCOW - XIII. A 2.4 per Cent Measurement of H0 from Lensed Quasars: 5.3sigma Tension between Early- and Late-Universe Probes". In: *Monthly Notices of the Royal Astronomical Society* 498 (1, 2019), pp. 1420–1439. DOI: 10.1093/mnras/stz3094 (cit. on p. 17).

[Yor+00] Donald G. York et al. "The Sloan Digital Sky Survey: Technical Summary". In: *The Astronomical Journal* 120 (1, 2000), pp. 1579–1587. DOI: 10.1086/301513 (cit. on p. 24).